ORNL/TM-11143

ornl

OAK RIDGE
NATIONAL
LABORATORY

MARTIN MARIETTA

Shield Optimization Program, Part I: Executive Summary

R. T. Santoro
T. A. Gabriel

OAK RIDGE NATIONAL LABORATORY
CENTRAL RESEARCH LIBRARY
CIRCULATION SECTION
4500N ROOM 175
LIBRARY LOAN COPY
DO NOT TRANSFER TO ANOTHER PERSON
If you wish someone else to see this report, send in name with report and the library will arrange a loan.

OPERATED BY
MARTIN MARIETTA ENERGY SYSTEMS, INC.
FOR THE UNITED STATES
DEPARTMENT OF ENERGY

This report has been reproduced directly from the best available copy.

Available to DOE and DOE contractors from the Office of Scientific and Technical Information, P.O. Box 62, Oak Ridge, TN 37831; prices available from (615) 576-8401, FTS 626-8401.

Available to the public from the National Technical Information Service, U.S. Department of Commerce, 5285 Port Royal Rd., Springfield, VA 22161.
NTIS price codes—Printed Copy: A04 Microfiche A01

This report was prepared as an account of work sponsored by an agency of the United States Government. Neither the United States Government nor any agency thereof, nor any of their employees, makes any warranty, express or implied, or assumes any legal liability or responsibility for the accuracy, completeness, or usefulness of any information, apparatus, product, or process disclosed, or represents that its use would not infringe privately owned rights. Reference herein to any specific commercial product, process, or service by trade name, trademark, manufacturer, or otherwise, does not necessarily constitute or imply its endorsement, recommendation, or favoring by the United States Government or any agency thereof. The views and opinions of authors expressed herein do not necessarily state or reflect those of the United States Government or any agency thereof.

ORNL/TM-11143

Engineering Physics and Mathematics Division

Shield Optimization Program, Part I: Executive Summary

R. T. Santoro and T. A. Gabriel

DATE PUBLISHED — June 1989

Prepared by the
OAK RIDGE NATIONAL LABORATORY
Oak Ridge, Tennessee 37831
operated by
MARTIN MARIETTA ENERGY SYSTEMS, INC.
for the
U.S. DEPARTMENT OF ENERGY
under contract DE-AC05-84OR21400

MARTIN MARIETTA ENERGY SYSTEMS LIBRARIES

3 4456 0299806 8

CONTENTS

ABSTRACT ix

1. INTRODUCTION 1

2. DETAILS OF THE CALCULATIONS AND SATELLITE GEOMETRY . 2

3. EFFECTS OF VAN ALLEN BELT RADIATION 8

3.1 RADIATION DAMAGE FROM VAN ALLEN BELT PROTONS . . 8

3.2 RADIATION DAMAGE FROM VAN ALLEN BELT ELECTRONS . 8

4. EFFECTS OF X–RAY RADIATION FROM NUCLEAR WEAPONS . 16

4.1 RESULTS FOR INCIDENT 2 KEV X–RAYS 16

5. EFFECTS OF NEUTRONS AND GAMMA RAYS FROM NUCLEAR WEAPONS 21

6. HYDRODYNAMIC RESPONSES OF MATERIALS FROM NUCLEAR WEAPON X–RAYS 26

6.1 HYDRODYNAMIC RESPONSE OF A BERYLLIUM TARGET TO MONO–ENERGETIC X–RAYS 26

6.2 COMPARISON OF THE THERMO–MECHANICAL RESPONSE OF AN ALUMINUM SLAB USING THE HULL AND PUFF–TFT CODES . 33

6.3 ENERGY DEPOSITION AT TIME = 0.0 33

6.4 COMPARISON OF RESULTS AT TIME = 0.1μsec. 33

7. CONCLUSIONS 39

REFERENCES 40

LIST OF FIGURES

Figure		Page
1	Calculational Model of the Space Based Interceptor Weapon Platform (a), with Interior views showing Launch Tube-Fuel Tanks Cluster (b), and the Central C^3 Bay (c)	3
2	Kinetic Kill Vehicle (a) and Exploded View of SBI Weapon Platform Showing KKVs Inside Launch Tubes (b)	4
3	Energy deposited as a function of depth for the 2 keV, 1 cal/cm^2 source incident upon the beryllium substrate (no surface impurity layer)	27
4	Energy deposited as a function of depth for the 2 keV, 1 cal/cm^2 source incident upon the 300 Å thick surface impurity layer with the base impurity concentrations	28
5	Energy deposited as a function of depth for the 2 keV, 1 cal/cm^2 source incident upon the 300 Å thick surface impurity layer with triple impurity concentrations	29
6	Temperature as a function of depth at specific times for the 2 keV, 1 cal/cm^2 source incident upon the beryllium substrate (no surface impurity layer)	30
7	Temperature as a function of depth at specific times for the 2 keV, 1 cal/cm^2 source incident upon the 300 Å thick surface impurity layer with the base impurity concentrations	31
8	Temperature as a function of depth at specific times for the 2 keV, 1 cal/cm^2 source incident upon the 300 Å thick surface impurity layer with triple impurity concentrations	32
9	Energy deposition as a function of depth	34
10	Density as a function of depth at 0.1μsec	36
11	Internal energy as a function of depth at 0.1μsec	37
12	Hydrostatic pressure versus depth at 0.1μsec	38

LIST OF TABLES

Table		Page
1	The Detector Regions Implemented in the Radiation Transport Analysis Routines	6
2	The Differential Proton Flux Spectrum in the Van Allen Belt for a Circular Orbit at an Altitude of 500 Kilometers	9
3	The Differential Electron Flux Spectrum in the Van Allen Belt for a Circular Orbit at an Altitude of 500 Kilometers	10
4	The Normalized Differential Electron Fluence Spectrum Due to a High–Altitude Nuclear Burst for a Circular Orbit at an Altitude of 500 Kilometers	11
5	Dose Due to Van Allen Belt Protons for a Circular Orbit at an Altitude of 500 Kilometers	12
6	Dose Due to Natural Background Van Allen Belt Electrons for a Circular Orbit at an Altitude of 500 Kilometers	13
7	Cumulative Dose Due to Nuclear Enhanced Van Allen Belt Electrons from a High–Altitude Nuclear Burst for a Circular Orbit at an Altitude of 500 Kilometers	14
8	Total Dose in rads (Si) Due to a 2 keV Temperature Blackbody X–Ray Source Located Directly Above the SBI Weapon Platform	17
9	Neutron and Gamma Dose Levels in the SBI Platform from the Deuterium–Tritium Fusion Source Positioned Directly Above the Solar Panels (rads·m^2/kTon)	22
10	Neutron and Gamma Dose Levels in the SBI Platform from the Fission Sources Positioned Directly Above the Platform Body (rads·m^2/kTon)	24
11	Approximate Mass Fractions by Phase	35

ABSTRACT

Detailed studies have been completed to estimate the radiation–induced damage in sensitive electronic components carried on a space–based interceptor weapons platform. The architecture of the interceptor was devised to be as realistic as possible. The analyses were completed for natural (Van Allen belt protons and electrons at an orbital altitude of 500 km) and man–made (nuclear weapons: neutrons, gamma–rays, X–rays, and pumped electron belts) radiation expected to be encountered by a SDI platform.

Studies have also been completed to determine the hydrodynamic responses of beryllium mirror surfaces to mono–energetic X–rays (1 and 2 keV). This work included the effects of impurities which are introduced into the surface during machining.

Finally, a comparison of the HULL and PUFF–TFT codes are presented which includes the thermo–mechanical response of an Al slab to 5 keV black body radiation.

1. INTRODUCTION

The Oak Ridge National Laboratory (ORNL) was tasked by the Air Force Weapons Laboratory (AFWL) to perform calculations to estimate the effects of natural and man–made radiation on a space deployed weapons platform having characteristics and components typical of those expected to be deployed as part of the Strategic Defense Initiative (SDI). This effort was funded and managed by the AFWL as part of the Spacecraft Armor Task Area of the SDIO Passive Survivability Technology Work Package Directive, WPD L004.*

A comprehensive series of radiation transport calculations were carried out to determine the effects of nuclear radiation on the critical components of a space deployed weapon platform. The resulting database can be used to assist platform designers in determining the disposition and composition of radiation shielding for critical systems and to also optimize the radiation protection characteristics of kinetic energy and laser weapon shields that will also be installed on the platform.

The work summarized here is a continuation of an earlier scoping study to determine the magnitude of the natural and man–made radiation effects on a satellite.[1] The original study, which was initiated three years ago, was carried out for a satellite that was approximated by a 1 m radius sphere having concentric layers of shielding surrounding a 0.02 m radius sphere. The interior sphere simulated a silicon based electronics package. In this study, a detailed representation of a weapons satellite (described below) was used. The calculated results summarized here are presented in five separate reports; three of which document the effects of natural (Van Allen Belt protons and electrons) and weapon radiation incident on the platform and the remainder of which summarize the results of the calculations of the hydrodynamic response of materials to x–radiation from nuclear weapon detonations.[2,3,4,5,6]

* WPD L004 is a program under the Survivability Office of the Key Technology Directorate of the SDIO Technology Deputate.

2. DETAILS OF THE CALCULATIONS AND SATELLITE GEOMETRY

The satellite geometry adopted for this study is shown in Figure 1a. The weapon platform, an ORNL Space Based Interceptor (SBI) concept is a cylindrical shell comprised of two interceptor–fuel tank (IFT) modules connected by a command, control, and communications (C^3) bay. Each IFT module contains five launch tube–kinetic–kill vehicle (KKV) assemblies and four fuel tanks. The platform has an overall length of 4.27 m and a diameter of 1.63 m. Figure 1b is an exploded view showing the interior of the platform and the orientation of the KKV launch tubes and the fuel tanks. Fuel is required for maneuvering the platform to evade space debris and enemy threats, perform station keeping, and for positioning the platform during engagement.

Power is supplied to the on–board electronics and electrical circuits by two solar panels, one on each side of the satellite. During conflict, the panels are folded along the top of the platform to reduce the cross–sectional area to enemy weapons. A shield to protect the platform from ground–based laser attack covers the surfaces of the platform that are exposed to the earth. A single antenna, mounted on the top of the platform, provides communication with sensor and battle management satellites.

Figure 1c shows the interior of the C^3 bay. The electronic packages are mounted in two concentric, thin–walled, ring–shaped containers. The central box houses the most sensitive electronics. The C^3 bay contains sufficient space to interpose additional shielding between critical electronic packages.

A prototypic KKV is shown in Figure 2a. The main components of the weapon are the warhead, guidance sensors, fuel tank, and the rocket motor. Figure 2b shows the KKV mounted inside of a launch tube.

The SBI weapon platform and KKV assemblies shown here were specifically designed for this study. The ORNL SBI concept is based on studies of architectures and reports and does not represent any actual system design. Many other components that might be found on such a system were not included. The principal concern was to represent subsystems that are

a. most sensitive to radiation damage, and

b. essential to a wartime mission.

The SBI platform, contents, solar panels, and KKV interceptors were modeled using the Combinatorial Geometry (CG) Package that is available for use with the Monte Carlo radiation transport codes HETC,[7] MORSE,[8] MICAP,[9] and EGS[10] which were used to estimate the effects of the various incident radiation. Figures 1 and 2 were, in fact, generated using the JUNEBUG[11] plotting package using the CG logic and descriptors as input.

Further details of the SBI platform and the CG logic may be found in Reference 3. In all of the calculations, the radiation damage was estimated at

ORNL-DWG 88-14286

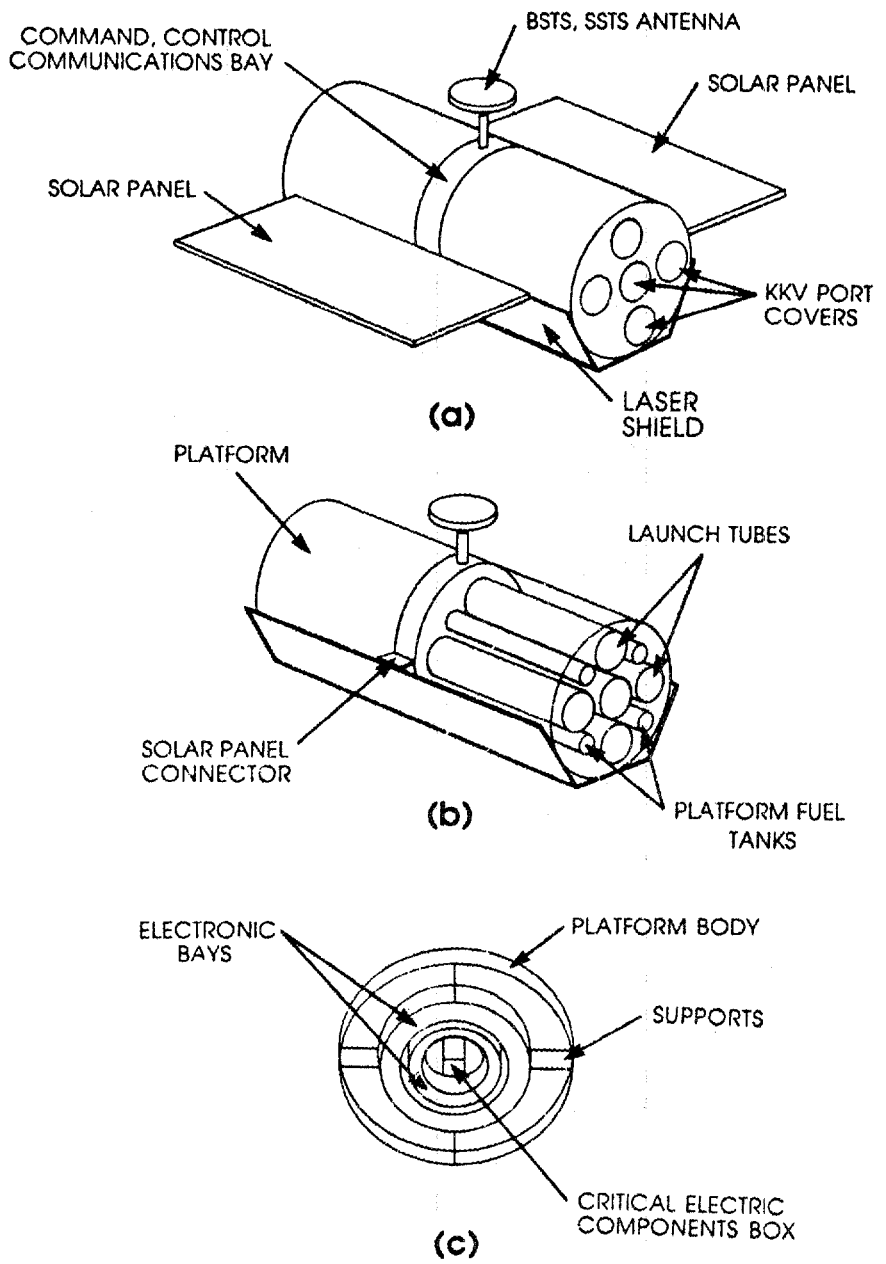

Figure 1. Calculational Model of the Space Based Interceptor Weapon Platform (a), with Interior views showing Launch Tube-Fuel Tanks Cluster (b), and the Central C^3 Bay (c).

ORNL-DWG 88-14287

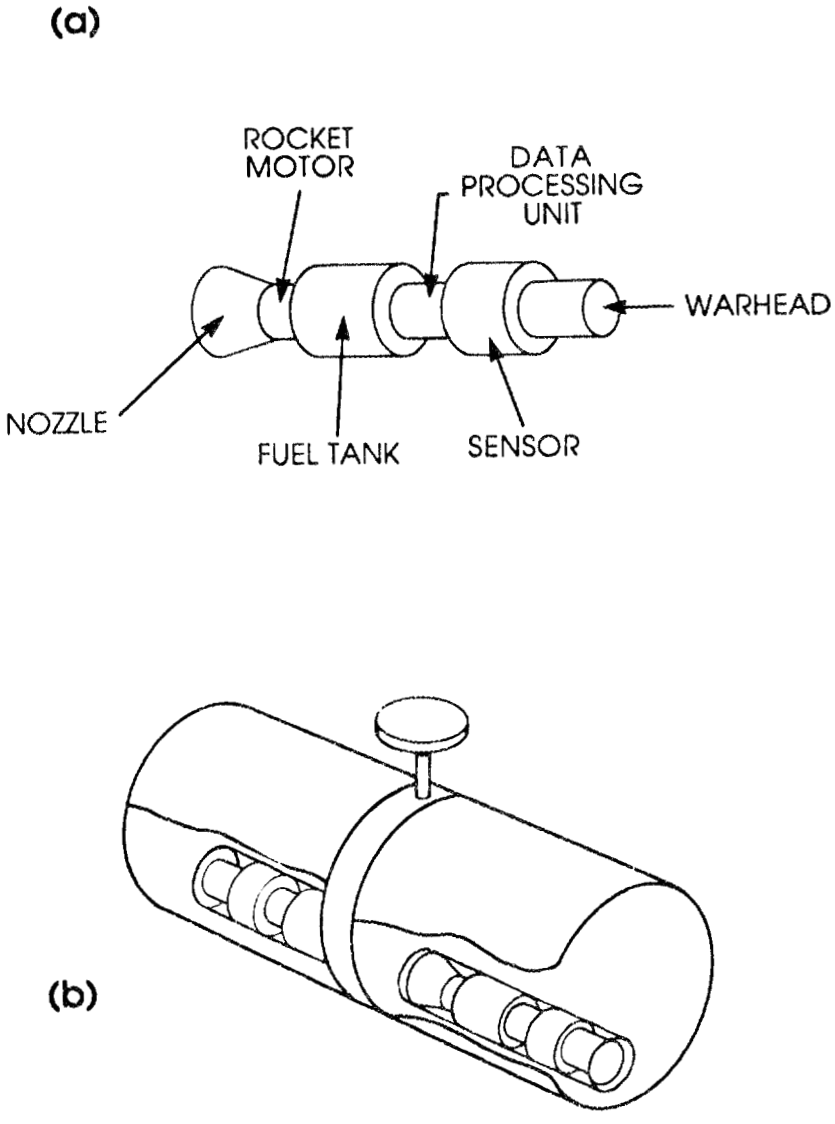

Figure 2. Kinetic Kill Vehicle (a) and Exploded View of SBI Weapon Platform Showing KKVs Inside Launch Tubes (b).

68 different detector locations. The term detector refers to a region in the CG representation in which an estimate of the radiation damage is desired. The locations of the detectors are summarized in Table 1.

The SBI was assumed to be in a circular orbit at an altitude of 500 kilometers and inclination angle of 0°. Future studies for satellites at other altitudes and inclinations, such as the Space Surveillance and Tracking System (SSTS) platforms, were to be carried out in future work. Also, more extensive work to further optimize shield assemblies to improve nuclear radiation threat mitigation were also planned.

Table 1

The Detector Regions Implemented in the Radiation Transport Analysis Routines

SBI Platform Component	Detector Region
C^3 Bay Critical Components Central Instrument Box	1
C^3 Bay Inner Instrument Ring	
0 to 60 Degree Segment	2
60 to 120 Degree Segment	3
120 to 180 Degree Segment	4
180 to 240 Degree Segment	5
240 to 300 Degree Segment	6
300 to 360 Degree Segment	7
C^3 Bay Outer Instrument Ring	
0 to 45 Degree Segment	8
45 to 90 Degree Segment	9
90 to 135 Degree Segment	10
135 to 180 Degree Segment	11
180 to 225 Degree Segment	12
225 to 270 Degree Segment	13
270 to 315 Degree Segment	14
315 to 360 Degree Segment	15
Kinetic Kill Vehicle Computers	
KKV Number 1	16
KKV Number 2	17
KKV Number 3	18
KKV Number 4	19
KKV Number 5	20
KKV Number 6	21
KKV Number 7	22
KKV Number 8	23
KKV Number 9	24
KKV Number 10	25
Kinetic Kill Vehicle Sensors	
KKV Number 1	26
KKV Number 2	27
KKV Number 3	28
KKV Number 4	29
KKV Number 5	30
KKV Number 6	31
KKV Number 7	32
KKV Number 8	33
KKV Number 9	34
KKV Number 10	35

Table 1 (Continued)

SBI Platform Component	Detector Region
Right Solar Panel	
Inner 0.5 cm Thick Shell	36
Next 0.5 cm Thick Shell	37
Next 0.5 cm Thick Shell	38
Next 0.5 cm Thick Shell	39
Outer 0.5 cm Thick Shell	40
Left Solar Panel	
Inner 0.5 cm Thick Shell	41
Next 0.5 cm Thick Shell	42
Next 0.5 cm Thick Shell	43
Next 0.5 cm Thick Shell	44
Outer 0.5 cm Thick Shell	45
BSTS, SSTS Antenna	
Inner 1.0 cm Thick Shell	46
Next 1.0 cm Thick Shell	47
Next 1.0 cm Thick Shell	48
Next 1.0 cm Thick Shell	49
Outer 1.0 cm Thick Shell	50
Kinetic Kill Vehicle Rocket Fuel Tanks	
KKV Number 1	51
KKV Number 2	52
KKV Number 3	53
KKV Number 4	54
KKV Number 5	55
KKV Number 6	56
KKV Number 7	57
KKV Number 8	58
KKV Number 9	59
KKV Number 10	60
SBI Weapon Platform Rocket Fuel Tanks	
SBI Tank Number 1	61
SBI Tank Number 2	62
SBI Tank Number 3	63
SBI Tank Number 4	64
SBI Tank Number 5	65
SBI Tank Number 6	66
SBI Tank Number 7	67
SBI Tank Number 8	68

3. EFFECTS OF VAN ALLEN BELT RADIATION

Calculations were carried out to determine the radiation damage from incident Van Allen belt proton and electron spectra and enhanced, or pumped, electron fluence spectra arising from the detonation of a Starfish–type nuclear weapon in space. The differential proton and electron flux spectra are summarized in Tables 2 and 3 and the differential pumped electron fluence spectrum is given in Table 4. For all of the spectra, the angular distribution of the radiation was taken to be isotropic. This is necessary because of the paucity of data and because any other representation would lead to erroneous results. The natural Van–Allen data were taken from the available references[12] and the pumped–belt spectra were provided by the AFWL.[13]

3.1 RADIATION DAMAGE FROM VAN ALLEN BELT PROTONS

The radiation damage to the various components of the satellite are summarized in Table 5. The column labeled "Primary" gives the dose from incident proton radiation only. The column labeled "Primary plus Secondary" is the dose from primary protons plus the dose from secondary particles produced by the reactions of the incident radiation with the materials in the SBI.

The dose/day from Van Allen protons in all 68 detector locations is small. Even after 10 years in orbit, the cumulative doses range from 200 rads in the C^3 bay to 1500 rads in the inner layers of the solar panel. These dose levels are well below the 1 megarad dose levels at which silicon–based electronic circuits and solar panel cells are expected to fail.

3.2 RADIATION DAMAGE FROM VAN ALLEN BELT ELECTRONS

The damage from VAB electrons and enhanced electron belt radiation in the SBI platform and KKVs at an altitude of 500 km is given in Tables 6 and 7, respectively. The damage from natural radiation is normalized to rads/day whereas the enhanced damage is in units of rads/electron.

Two trends are evident in the data presented in Tables 6 and 7. First is the dose as a function of depth in the solar panels and the antenna. The low energy natural electron spectrum results predominately in a surface dose in the components. The dose then falls off rapidly with depth. Any damage to components inside of the platform can result only from secondary bremsstrahlung photons produced from primary electron interactions. The enhanced electron spectrum also leads to a large surface dose. However, since the electrons are somewhat more energetic and the spectrum is harder, the dose profile in these components is much flatter and the dose in the interior layers is significantly higher than the dose due to the natural electron environment. The second trend is the magnitude of the dose produced by the two radiation modes. Comparing the dose averaged through the solar panel reveals that the dose rate from the natural environment is 2.29×10^{-3} rad/day whereas the enhanced electron dose rate at six hours after weapon detonation is 1.1×10^3 rads/day. The slow decay of the enhanced spectrum indicates that the

Table 2

The Differential Proton Flux Spectrum in the Van Allen Belt for a Circular Orbit at an Altitude of 500 Kilometers

Energy (MeV)	Differential Flux (protons/cm^2 · MeV · day)	Energy (MeV)	Differential Flux (protons/cm^2 · MeV · day)
30	4.400+04[a]	500	8.360+01
40	3.983+04	520	6.475+01
50	3.520+04	540	5.034+01
60	2.843+04	560	3.929+01
70	2.316+04	580	3.078+01
80	1.904+04	600	2.420+01
90	1.578+04	620	1.901+01
100	1.320+04	640	1.503−01
120	9.429+03	660	1.195−01
140	7.025+03	680	9.563+00
160	5.642+03	700	7.700+00
180	4.649+03	720	6.364+00
200	3.740+03	740	5.240+00
220	2.746+03	760	4.298+00
240	2.036+03	780	3.513+00
260	1.525+03	800	2.860+00
280	1.153+03	820	2.279+00
300	8.800+02	840	1.825+00
320	6.887+02	860	1.470+00
340	5.401+02	880	1.190+00
360	4.246+02	900	9.680−01
380	3.344+02	920	7.919−01
400	2.640+02	940	6.513−01
420	2.113+02	960	5.385−01
440	1.685+02	980	4.476−01
460	1.339+02	1000	3.740−01
480	1.060+02		

[a]Read as 4.400×10^4.

Table 3

The Differential Electron Flux Spectrum in the Van Allen Belt for a Circular Orbit at an Altitude of 500 Kilometers

Energy (MeV)	Differential Flux (electrons/cm^2 · MeV · day)	Energy (MeV)	Differential Flux (electrons/cm^2 · MeV · day)
0.05	4.320+10[a]	2.60	1.642+07
0.10	2.592+10	2.80	1.296+07
0.20	1.152+10	3.00	1.008+07
0.30	5.184+09	3.20	5.760+06
0.40	2.448+09	3.40	3.456+06
0.50	1.296+09	3.60	1.872+06
0.60	8.064+08	3.80	9.792+05
0.70	5.760+08	4.00	5.184+05
0.80	4.608+08	4.20	2.880+05
0.90	3.456+08	4.40	1.642+05
1.00	2.448+08	4.60	9.504+04
1.20	1.642+08	4.80	5.184+04
1.40	1.123+08	5.00	2.880+04
1.60	7.776+07	6.00	1.584+03
1.80	5.760+07	7.00	9.504+01
2.00	4.032+07	8.00	5.184+00
2.20	2.880+07	9.00	2.880−01
2.40	2.102+07	10.00	1.526−01

[a]Read as 4.320×10^{10}.

Table 4

The Normalized Differential Electron Fluence Spectrum Due to a High–Altitude Nuclear Burst for a Circular Orbit at an Altitude of 500 Kilometers

Lower Energy (MeV)	Differential Fluence (electrons/cm^2)
0.04	6.66–03[a]
0.25	5.40–02
0.50	1.28–01
1.00	3.45–01
2.00	2.66–01
3.00	1.28–01
4.00	4.73–02
5.00	1.78–02
6.00	6.19–03
7.00	1.65–03
10.00	—

[a]Read as 6.66×10^{-3}.

Table 5

Dose Due to Van Allen Belt Protons for a Circular Orbit at an Altitude of 500 Kilometers

Detector Region	Primary[a] (rads/day)	Primary & Secondary[b] (rads/day)
C^3 Bay Central Instrument Box	4.74−02 ± 10%	4.89−02[c] ± 16%
C^3 Bay Inner Instrument Ring	4.90−02 ± 3%	4.34−02 ± 4%
C^3 Bay Outer Instrument Ring	6.89−02 ± 3%	6.26−02 ± 3%
Average for the Kinetic Kill Vehicle Computers	6.28−02 ± 4%	6.61−02 ± 5%
Average for the Kinetic Kill Vehicle Sensors	7.63−02 ± 3%	7.07−02 ± 4%
Inner 0.5 cm Thickness of the Solar Panels	4.14−01 ± 2%	4.10−01 ± 2%
Next 0.5 cm Thickness of the Solar Panels	1.75−01 ± 3%	1.71−01 ± 4%
Next 0.5 cm Thickness of the Solar Panels	2.12−01 ± 3%	2.01−01 ± 3%
Next 0.5 cm Thickness of the Solar Panels	2.39−01 ± 2%	2.43−01 ± 2%
Outer 0.5 cm Thickness of the Solar Panels	1.05−01 ± 3%	1.17−01 ± 4%
Average for the Solar Panels	1.85−01 ± 1%	2.13−01 ± 1%
Inner 1.0 cm Thickness of the BSTS, SSTS Antenna	3.22−01 ± 6%	3.30−01 ± 12%
Next 1.0 cm Thickness of the BSTS, SSTS Antenna	1.51−01 ± 13%	1.57−01 ± 17%
Next 1.0 cm Thickness of the BSTS, SSTS Antenna	2.13−01 ± 10%	1.97−01 ± 9%
Next 1.0 cm Thickness of the BSTS, SSTS Antenna	2.04−01 ± 8%	2.29−01 ± 8%
Outer 1.0 cm Thickness of the BSTS, SSTS Antenna	1.22−01 ± 13%	1.12−01 ± 10%
Average for the BSTS, SSTS Antenna	1.96−01 ± 4%	1.64−01 ± 5%
Average for the Kinetic Kill Vehicle Rocket Fuel	7.94−02 ± 2%	7.31−02 ± 3%
Average for the SBI Weapon Platform Rocket Fuel	6.85−02 ± 2%	6.42−02 ± 2%

[a] Dose due to unattenuated primary protons only.
[b] Dose due to primary and secondary collisions and full proton transport.
[c] Read as 4.89×10^{-2}.

Table 6

Dose Due to Natural Background Van Allen Belt Electrons for a Circular Orbit at an Altitude of 500 Kilometers

Detector Region	Natural Background Dose (rads/day)	Natural Background Dose After Ten Years (rads)
C^3 Bay Central Instrument Box	3.23−05[a] ± 30%	1.18−01 ± 30%
C^3 Bay Inner Instrument Ring	5.19−05 ± 15%	1.90−01 ± 15%
C^3 Bay Outer Instrument Ring	1.49−04 ± 12%	5.44−01 ± 12%
Average for the Kinetic Kill Vehicle Computers	7.39−05 ± 15%	2.70−01 ± 15%
Average for the Kinetic Kill Vehicle Sensors	1.20−04 ± 11%	4.38−01 ± 11%
Inner 0.5 cm Thickness of the Solar Panels	5.71−04 ± 14%	2.09+00 ± 14%
Next 0.5 cm Thickness of the Solar Panels	3.25−03 ± 3%	1.19+00 ± 3%
Next 0.5 cm Thickness of the Solar Panels	3.10−02 ± 2%	1.13+02 ± 2%
Next 0.5 cm Thickness of the Solar Panels	2.26−01 ± 2%	8.25+02 ± 2%
Outer 0.5 cm Thickness of the Solar Panels	8.78+00 ± 2%	3.21+04 ± 2%
Average for the Solar Panels	2.29−03 ± 3%	8.36+00 ± 3%
Inner 1.0 cm Thickness of the BSTS, SSTS Antenna	5.17−04 ± 33%	1.89+00 ± 33%
Next 1.0 cm Thickness of the BSTS, SSTS Antenna	4.19−04 ± 26%	1.53+00 ± 26%
Next 1.0 cm Thickness of the BSTS, SSTS Antenna	5.87−03 ± 12%	2.14+01 ± 12%
Next 1.0 cm Thickness of the BSTS, SSTS Antenna	7.29−02 ± 6%	2.66+02 ± 6%
Outer 1.0 cm Thickness of the BSTS, SSTS Antenna	6.23+00 ± 10%	2.28+04 ± 10%
Average for the BSTS, SSTS Antenna	5.83−04 ± 2%	2.13+00 ± 2%
Average for the Kinetic Kill Vehicle Rocket Fuel	1.02−04 ± 11%	3.73−01 ± 11%
Average for the SBI Weapon Platform Rocket Fuel	3.51−04 ± 7%	1.28+00 ± 7%

[a]Read as 3.23×10^{-5}.

Table 7

Cumulative Dose Due to Nuclear Enhanced Van Allen Belt Electrons from a High-Altitude Nuclear Burst for a Circular Orbit at an Altitude of 500 Kilometers

Detector Region	Cumulative Dose After High Altitude Nuclear Weapon Burst[a] (rads)							
	6 Hrs	1 Day	2 Days	7 Days	30 Days	60 Days	180 Days	1 Year
C^3 Bay Central Instrument Box	8.80−01[b]	2.73+00	5.17+00	1.43+01	3.50+01	5.50+01	1.08+02	1.60+02
C^3 Bay Inner Instrument Ring	2.95+00	9.16+00	1.73+01	4.80+01	1.17+02	1.85+02	3.62+02	5.38+02
C^3 Bay Outer Instrument Ring	5.34+00	1.66+01	3.14+01	8.69+01	2.12+02	3.34+02	6.55+02	9.74+02
Average for the Kinetic Kill Vehicle Computers	3.21+00	9.97+00	1.89+01	5.22+01	1.28+02	2.01+02	3.94+02	5.86+02
Average for the Kinetic Kill Vehicle Sensors	5.00+00	1.55+01	2.94+01	8.14+01	1.99+02	3.13+02	6.13+02	9.12+02
Inner 0.5 cm Thickness of the Solar Panels	2.07+02	6.41+02	1.21+03	3.36+03	8.21+03	1.29+04	2.53+04	3.77+04
Next 0.5 cm Thickness of the Solar Panels	4.41+02	1.37+03	2.59+03	7.17+03	1.75+04	2.76+04	5.41+04	8.04+04
Next 0.5 cm Thickness of the Solar Panels	1.17+03	3.64+03	6.89+03	1.91+04	4.67+04	7.34+04	1.44+05	2.14+05
Next 0.5 cm Thickness of the Solar Panels	3.12+03	9.67+03	1.83+04	5.06+04	1.24+05	1.95+05	3.82+05	5.68+05
Outer 0.5 cm Thickness of the Solar Panels	7.64+03	2.37+04	4.49+04	1.24+05	3.04+05	4.78+05	9.36+05	1.39+06
Average for the Solar Panels	2.79+02	8.67+02	1.64+03	4.54+03	1.11+04	1.75+04	3.43+04	5.09+04
Inner 1.0 cm Thickness of the BSTS, SSTS Antennna	5.33+01	1.65+02	3.13+02	8.67+02	2.12+03	3.34+03	6.53+03	9.72+03
Next 1.0 cm Thickness of the BSTS, SSTS Antenna	1.25+02	3.87+02	7.33+02	2.03+03	4.96+03	7.81+03	1.53+04	2.28+04
Next 1.0 cm Thickness of the BSTS, SSTS Antenna	3.78+02	1.17+03	2.22+03	6.15+03	1.50+04	2.37+04	4.64+04	6.90+04
Next 1.0 cm Thickness of the BSTS, SSTS Antenna	1.39+03	4.32+03	8.17+03	2.26+04	5.53+04	8.71+04	1.71+05	2.54+05
Outer 1.0 cm Thickness of the BSTS, SSTS Antenna	6.05+03	1.88+04	3.55+04	9.84+04	2.41+05	3.79+05	7.42+05	1.10+06
Average for the BSTS, SSTS Antenna	6.74+01	2.09+02	3.95+02	1.09+03	2.68+03	4.21+03	8.26+03	1.23+04
Average for the Kinetic Kill Vehicle Rocket Fuel	4.07+00	1.26+01	2.39+01	6.62+01	1.62+02	2.55+02	4.99+02	7.42+02
Average for the SBI Weapon Platform Rocket Fuel	1.19+01	3.68+01	6.96+01	1.93+02	4.71+02	7.42+02	1.45+03	2.16+03

[a] Excludes natural background electron dose.
[b] Read as 8.80×10^{-1}.

dose accumulated in the outer layers of the solar panels and antenna is sufficiently large to cause material damage and bit upset, degradation, and failure in near surface mounted electronic components.

To determine the combined dose from both environments, the dose rate from the natural environment must be multiplied by the time that the platform resided in the environment and added to the cumulative dose from enhancement. For example, if the platform was in orbit for one year prior to the detonation of a weapon in space, the dose average with depth in the solar panels would be 0.84 rads from natural electrons and 67.5 rads from protons. Six hours after the explosion, the dose from enhanced electrons would be 279 rads. Additional data may be found in Reference 2.

4. EFFECTS OF X–RAY RADIATION FROM NUCLEAR WEAPONS

The dose to the components of the SBI platform was also calculated for incident x–rays produced from the detonation of a nuclear weapon in space. At detonation, the material comprising the weapon is heated to tens of millions of degrees Kelvin. At high temperature, blackbody radiation occurs in the form of x–rays with approximately 75% of the total energy being emitted in the form of x–radiation. Since the weapon is exploded in space, the only attenuation is geometric and the platform is exposed to x–ray fluences sufficient to cause damage to the sensitive components of the platform.

Calculations using the EGS4 Monte Carlo code[10] were carried out for several incident blackbody cold ($\lesssim$2 keV) and hot ($\gtrsim$2 keV) x–ray spectra. The differential energy distributions (x–rays/unit energy) were calculated using the relation

$$\frac{dN(E,kT)}{dE} = \frac{CE^2}{e^{E/kT}-1} \tag{1}$$

where N is the number of x–rays with energy E about dE, kT is the temperature of the radiation emitting body, and C is a normalization factor.[14] X–ray damage to the SBI was estimated for values of kT of 2, 5, 10, and 20 keV. As the temperature of the blackbody emitter increases, the emission spectrum hardens. For the temperatures considered, the average energy of the emitted x–rays corresponds to 5.38, 13.5, 27.0, and 53.9 keV. Surface loadings between 1–10 cal/cm^2 were considered.

Since the origin of the nuclear explosion with respect to the satellite is uncertain, three scenarios were studied; a weapon detonated directly above the SBI, a detonation directly ahead of the satellite, and a burst above and in front of the SBI at an angle of 45°. The radiation from the burst was taken to be omnidirectional. The radiation damage is given in units of rad(Si).

4.1 RESULTS FOR INCIDENT 2 KEV X–RAYS

The doses in the components of the SBI (See Table 1) from 2 keV x–rays emitted from a weapon detonated directly above the satellite are summarized in Table 8 as a function of external wall loadings of 1, 2, 5, and 10 cal/cm^2. Data for other blackbody temperatures and weapon orientations are presented and discussed in detail in Reference 3.

Symmetry with respect to the source of radiation was used whenever possible to reduce the fractional standard deviation (FSD) in the calculated results. Where the FSD values are larger than approximately 15%, which is considered as statistically acceptable for Monte Carlo results, the estimated data should be taken to be relative magnitudes of the absorbed dose and not as absolute values. Attempts to reduce the FSD values at all locations would result in unacceptable calculational times with no significant difference in the dose values.

For 2 keV radiation, the damage in most of the components of the SBI is small at all wall loadings. Excessive damage does, however, occur in detector regions 40,

Table 8

Total Dose in rads (Si) due to a 2 keV Temperature Blackbody X-Ray Source Located Directly Above the SBI Weapon Platform

Detector Region	Exterior Wall Loading 1 cal/cm^2	2 cal/cm^2	5 cal/cm^2	10 cal/cm^2	% FSD
1	0.000+00	0.000+00	0.000+00	0.000+00	0.0
2	0.000+00	0.000+00	0.000+00	0.000+00	0.0
3	0.000+00	0.000+00	0.000+00	0.000+00	0.0
4	0.000+00	0.000+00	0.000+00	0.000+00	0.0
5	0.000+00	0.000+00	0.000+00	0.000+00	0.0
6	0.000+00	0.000+00	0.000+00	0.000+00	0.0
7	0.000+00	0.000+00	0.000+00	0.000+00	0.0
8	7.836−05[a]	1.567−04	3.918−04	7.836−04	58.9
9	0.000+00	0.000+00	0.000+00	0.000+00	0.0
10	0.000+00	0.000+00	0.000+00	0.000+00	0.0
11	7.836−05	1.567−04	3.918−04	7.836−04	58.9
12	2.148−02	4.297−02	1.074−01	2.148−01	16.5
13	8.294−03	1.659−02	4.147−02	8.294−02	26.2
14	8.294−03	1.659−02	4.147−02	8.294−02	26.2
15	2.148−02	4.297−02	1.074−01	2.148−01	16.5
16	7.568−05	1.514−04	3.784−04	7.568−04	49.9
17	0.000+00	0.000+00	0.000+00	0.000+00	0.0
18	4.532−02	9.065−02	2.266−01	4.532−01	13.7
19	6.367−03	1.273−02	3.183−02	6.367−02	16.1
20	6.367−03	1.273−02	3.183−02	6.367−02	16.1
21	7.568−05	1.514−04	3.784−04	7.568−04	49.9
22	0.000+00	0.000+00	0.000+00	0.000+00	0.0
23	4.532−02	9.065−02	2.266−01	4.532−01	13.7
24	6.367−03	1.273−02	3.183−02	6.367−02	16.1
25	6.367−03	1.273−02	3.183−02	6.367−02	16.1
26	9.484−04	1.897−03	4.742−03	9.484−03	99.9
27	0.000+00	0.000+00	0.000+00	0.000+00	0.0
28	2.256−02	4.512−02	1.128−01	2.256−01	12.1
29	3.021−03	6.043−03	1.511−02	3.021−02	14.7
30	3.021−03	6.043−03	1.511−02	3.021−02	14.7
31	9.484−04	1.897−03	4.742−03	9.484−03	99.9
32	0.000+00	0.000+00	0.000+00	0.000+00	0.0
33	2.256−02	4.512−02	1.128−01	2.256−01	12.1
34	3.021−03	6.043−03	1.511−02	3.021−02	14.7
35	3.021−03	6.043−03	1.511−02	3.021−02	14.7

[a]Read as 7.836×10^{-5}.

Table 8 - continued

Detector Region	Exterior Wall Loading 1 cal/cm^2	2 cal/cm^2	5 cal/cm^2	10 cal/cm^2	% FSD
36	4.032+01	8.064+01	2.016+02	4.032+02	5.9
37	6.243+01	1.249+02	3.122+02	6.243+02	5.2
38	1.063+02	2.126+02	5.314+02	1.063+03	4.0
39	2.958+02	5.916+02	1.479+03	2.958+03	3.2
40	3.608+03	7.215+03	1.804+04	3.608+04	0.5
41	4.032+01	8.064+01	2.016+02	4.032+02	5.9
42	6.243+01	1.249+02	3.122+02	6.243+02	5.2
43	1.063+02	2.126+02	5.314+02	1.063+03	4.0
44	2.958+02	5.916+02	1.479+03	2.958+03	3.2
45	3.608+03	7.215+03	1.804+04	3.608+04	0.5
46	5.626−01	1.125+00	2.813+00	5.626+00	12.7
47	9.036−01	1.807+00	4.518+00	9.036+00	11.4
48	2.207+00	4.415+00	1.104+01	2.207+01	9.1
49	1.388+01	2.776+01	6.939+01	1.388+02	6.1
50	3.623+03	7.246+03	1.812+04	3.623+04	1.6
51	3.033−06	6.066−06	1.516−05	3.033−05	84.1
52	0.000+00	0.000+00	0.000+00	0.000+00	0.0
53	1.737−02	3.473−02	8.684−02	1.737−01	13.1
54	2.017−03	4.033−03	1.008−02	2.017−02	15.2
55	2.017−03	4.033−03	1.008−02	2.017−02	15.2
56	3.033−06	6.066−06	1.516−05	3.033−05	84.1
57	0.000+00	0.000+00	0.000+00	0.000+00	0.0
58	1.737−02	3.473−02	8.684−02	1.737−01	13.1
59	2.017−03	4.033−03	1.008−02	2.017−02	15.2
60	2.017−03	4.033−03	1.008−02	2.017−02	15.2
61	2.249−06	4.498−06	1.124−05	2.249−05	35.2
62	2.249−06	4.498−06	1.124−05	2.249−05	35.2
63	3.779−02	7.559−02	1.890−01	3.779−01	5.2
64	3.779−02	7.559−02	1.890−01	3.779−01	5.2
65	2.249−06	4.498−06	1.124−05	2.249−05	35.2
66	2.249−06	4.498−06	1.124−05	2.249−05	35.2
67	3.779−02	7.559−02	1.890−01	3.779−01	5.2
68	3.779−02	7.559−02	1.890−01	3.779−01	5.2

45, and 50, which correspond to the outer layers of the solar panels and the antenna. A surprise detonation of a weapon could result in total loss of power (except for battery backup) and loss of capability to communicate with battle management and adjacent systems.

The damage in all of the detector regions of the SBI increases with increasing x–ray energy independent of the location of the explosion. The damage to the components increases as a function of depth because of the greater penetrating capability of the more energetic x–rays. For 20 keV radiation, for example, the dose in most of the components is of the order of hundreds of rads (Si) compared to millirad values for the results shown in Table 8. In the work reported in Reference 3, calculations were performed for monoenergetic incident radiation. In a realistic weapon detonation, the x–radiation would be emitted at several energies. The dose at wall loading, w, received by any component, can be determined by weighting the monoenergetic results given in Reference 3 with an expression of the form

$$D(w) = \Sigma F(E, w) * D(E, w) \ , \tag{2}$$

where $F(E, w)$ is the fraction of emitted x–rays having energy E and $D(E, w)$ is the dose in the particular component from x–rays of energy E.

The majority of radiation from a nuclear weapon is in the form of X–rays which impact on the surface of the platform in the form of an energetic hydrodynamic-like impulse and, depending on the blackbody temperature of the weapon, deliver large doses to on-board electronic equipment. Surface damage will generally predominate. The single event upset and latch-up rates in vital circuits from nuclear weapon X–ray radiation may cause mission failure for weapon platforms that are near the limit of the wall loadings suggested (less than 10 cal/cm^2). The solar panels and the BSTS, SSTS antenna dose profiles exhibit a sharp decline at the lower temperature spectra (four orders of magnitude at 1 keV) and relatively flat distributions at the higher temperature spectra (less than 20% at 20 keV). The dose to the outer shell of the solar panels and antenna for the 1, 2, and 5 keV devices is sufficiently large enough to cause permanent damage to the electronics. Further analysis needs to be performed to determine surface effects (blow–off, melting, etc.) for the 1, 2, and 5 keV source spectra.

The dose to the sensitive components within the exterior hull of the platform was not sufficient to cause any damage at a 1 cal/cm^2 exterior wall loading. At higher wall loadings, some of the KKV computers and sensors begin to receive doses large enough to cause damage. Furthermore, the majority of the dose to the internal components of the SBI platform came from blackbody devices with temperatures greater than 10 keV. The low temperature devices will yield a higher flux of X–rays, but the incident energy will be insufficient to cause permanent damage to the internal electronic components.

The analysis presented in this work focused on the total dose (in units of rads or rads $\cdot$ cm^2/X-ray) received by the various components on board the SBI weapon platform without regard to the rate at which the dose was received. As stated above, generally the total dose to the sensitive components within the exterior hull

of the platform was not sufficient enough to cause any damage at a 1 cal/cm^2 exterior wall loading. However, a typical weapon detonation releases the X-ray radiation in a pulse with a width on the order of 10–40 nanosecond. Therefore, if a 40 nanosecond pulse width is assumed, all of the total dose results would have to be multiplied by 2.5×10^7 sec^{-1} to obtain the dose rate (Gamma dot) results. This would yield dose rates to the sensitive components in the range of 10^8–10^{12} rads/sec which could be large enough to cause damage. Consequently, the dose rate becomes the primary mode of failure even though the total dose is not large enough to cause any damage to the sensitive components. In this case, additional shielding around the sensitive components would be required.

5. EFFECTS OF NEUTRONS AND GAMMA RAYS FROM NUCLEAR WEAPONS

The neutron and gamma–ray induced radiation damage in the components of the SBI was calculated using the Monte Carlo code MORSE[8] for three nuclear weapon spectra: a deuterium—tritium fusion reaction, ^{235}U reaction, and prompt fission gamma rays. As in the weapon x–ray analysis, the doses were obtained for detonations directly above the satellite, in front of the SBI, and above and in front of the satellite at an angle of 45°. The calculations were carried out using 500,000 source particle histories which, in general, yielded excellent fractional standard deviations in the calculated results. The doses were normalized to a one kiloton yield of neutrons and gamma–rays assuming 100% efficiency in weapon yield. This assumption results in 1.88×10^{23} fusion neutrons and 1.06×10^{24} prompt fission gamma rays, or 1.49×10^{24} fusion neutrons per kiloton of weapon yield. The damage data are presented in units of rads (material) $*m^2$/kTon. The dose to a particular component is obtained by multiplying by the weapon yield and dividing by the square of the distance from the explosion to the satellite. (The geometric factor 4π has been included in the numerical results.)

The dose in the components of the SBI were calculated for the separate weapon spectra described above. However, an actual weapon spectrum is a combination of the fusion and fission spectra which can be modeled by appropriately combining the data given in Reference 4. Gamma–ray contributions may range from 35% for a fusion weapon to 95% for a fission device.

The results for fusion and fission weapons detonated directly above the SBI are summarized in Tables 9 and 10, respectively. The damage data are given for the 68 detector regions summarized in Table 1. Results for other weapon orientations are summarized in Reference 4.

The total dose level in a component is a summation of the contributions from the primary and secondary particles. For example, a 100 kTon fission device detonated at 1 kilometer above the SBI platform generates a total dose in the central instrument box of 26.5 krad(Si) from primary neutrons, primary gamma rays (prompt gamma rays), and secondary gamma rays.

The results in Tables 9 and 10 can be normalized to X–ray surface loadings. If it is assumed that 75% of the energy from a detonation is in the form of X–rays, then device yields may be converted to surface loadings (using 10^{12} cal/kT). For example, the 1962 Starfish event had a yield of 1.4 MT, of which 1 MT was fission yield. At a distance of 91.4 km from the device, the surface loading is 1 cal/cm^2. Using this distance and yield, coupled with the source spectra given in these tables, total dose and dose rate can be calculated for the SBI model.

Electronic devices can be hardened to withstand high levels of neutron fluence and dose. Therefore, the gamma dose level and dose rate predominates in terms of electronic component shielding. An actual weapon spectrum may be a combination of fusion and fission components, which can be modeled using the spectra in Reference 4. By adding some high–Z material around the central instrument bay, significant reductions in gamma dose may be obtained.

Table 9

Neutron and Gamma Dose Levels in the SBI Platform from the Deuterium–Tritium Fusion Source Positioned Directly Above the Solar Panels (rads·m^2/kTon)[a]

	Neutron	Secondary Gamma
1	8.032+06[b] ± 0.530[c]	1.523+07 ± 0.401
2	9.629+06 ± 0.381	1.231+07 ± 0.264
3	1.235+07 ± 0.407	1.589+07 ± 0.305
4	1.322+07 ± 0.361	2.688+07 ± 0.414
5	1.564+07 ± 0.297	1.562+07 ± 0.433
6	2.096+07 ± 0.303	2.141+07 ± 0.265
7	1.175+07 ± 0.313	3.503+07 ± 0.380
8	2.180+07 ± 0.257	1.547+07 ± 0.214
9	3.425+07 ± 0.303	1.172+07 ± 0.346
10	3.432+07 ± 0.277	1.694+07 ± 0.499
11	2.210+07 ± 0.223	2.799+07 ± 0.275
12	1.772+07 ± 0.261	1.835+07 ± 0.203
13	1.033+07 ± 0.418	8.380+06 ± 0.236
14	2.582+07 ± 0.282	3.230+07 ± 0.482
15	2.060+07 ± 0.175	1.890+07 ± 0.214
16	5.140+06 ± 0.539	6.419+06 ± 0.304
17	1.059+07 ± 0.358	9.037+06 ± 0.488
18	2.407+06 ± 0.294	9.172+06 ± 0.288
19	3.996+06 ± 0.432	7.493+06 ± 0.336
20	1.032+07 ± 0.335	1.352+07 ± 0.316
21	3.745+06 ± 0.404	1.118+07 ± 0.348
22	4.590+06 ± 0.527	2.548+07 ± 0.356
23	7.158+06 ± 0.437	7.688+06 ± 0.254
24	7.731+06 ± 0.422	1.151+07 ± 0.282
25	1.161+07 ± 0.306	1.311+07 ± 0.256
26	5.647+06 ± 0.373	7.285+06 ± 0.376
27	3.831+06 ± 0.343	1.086+07 ± 0.290
28	6.811+06 ± 0.345	7.972+06 ± 0.250
29	1.131+07 ± 0.330	1.392+07 ± 0.333
30	8.115+06 ± 0.350	7.882+06 ± 0.401
31	7.958+06 ± 0.389	1.209+07 ± 0.289
32	7.930+06 ± 0.311	1.343+07 ± 0.287
33	8.819+06 ± 0.299	4.087+06 ± 0.328
34	9.775+06 ± 0.347	9.827+06 ± 0.284

[a]A factor of 4π has already been included in these values.
[b]Read as 8.032×10^6.
[c]Fractional Standard Deviation.

Table 9 (Continued)

	Neutron	Secondary Gamma
35	9.118+06 ± 0.350	4.228+06 ± 0.227
36	5.404+09 ± 0.004	7.195+07 ± 0.033
37	7.811+08 ± 0.009	6.255+07 ± 0.042
38	6.165+08 ± 0.010	4.672+07 ± 0.035
39	4.331+08 ± 0.010	3.340+07 ± 0.035
40	2.007+08 ± 0.013	1.344+07 ± 0.056
41	5.415+09 ± 0.003	7.008+07 ± 0.039
42	7.551+08 ± 0.009	6.162+07 ± 0.037
43	6.225+08 ± 0.010	4.518+07 ± 0.044
44	4.295+08 ± 0.009	3.606+07 ± 0.043
45	2.022+08 ± 0.015	1.333+07 ± 0.047
46	1.508+08 ± 0.139	5.423+07 ± 0.189
47	2.653+07 ± 0.186	2.128+07 ± 0.285
48	1.977+07 ± 0.190	1.489+07 ± 0.573
49	1.494+07 ± 0.184	7.100+06 ± 0.252
50	7.178+06 ± 0.234	2.012+06 ± 0.281
51	5.716+08 ± 0.180	2.931+07 ± 0.221
52	8.054+08 ± 0.158	3.522+07 ± 0.169
53	7.603+08 ± 0.153	2.844+07 ± 0.172
54	1.278+09 ± 0.132	3.468+07 ± 0.198
55	9.089+08 ± 0.160	3.969+07 ± 0.210
56	7.034+08 ± 0.176	2.504+07 ± 0.194
57	9.663+08 ± 0.158	4.534+07 ± 0.247
58	7.005+08 ± 0.157	2.641+07 ± 0.183
59	1.086+09 ± 0.137	2.909+07 ± 0.173
60	9.188+08 ± 0.181	3.002+07 ± 0.260
61	3.229+09 ± 0.108	1.277+08 ± 0.108
62	3.056+09 ± 0.096	1.458+08 ± 0.103
63	4.316+09 ± 0.091	1.471+08 ± 0.106
64	3.892+09 ± 0.090	1.393+08 ± 0.094
65	3.093+09 ± 0.123	1.732+08 ± 0.175
66	3.197+09 ± 0.109	1.826+08 ± 0.161
67	4.693+09 ± 0.087	1.542+08 ± 0.103
68	4.370+09 ± 0.088	1.411+08 ± 0.088

Table 10

Neutron and Gamma Dose Levels in the SBI Platform from the Fission Sources Positioned Directly Above the Platform Body (rads·m²/kTon)[a]

	Neutron	Secondary Gamma	Prompt Gamma
1	1.622+07[b] ± 0.038[c]	1.693+07 ± 0.086	2.323+08 ± 0.034
2	1.683+07 ± 0.035	1.908+07 ± 0.117	2.762+08 ± 0.050
3	1.530+07 ± 0.028	1.705+07 ± 0.078	2.357+08 ± 0.035
4	1.332+07 ± 0.037	1.706+07 ± 0.065	1.969+08 ± 0.044
5	2.173+07 ± 0.028	1.988+07 ± 0.058	3.852+08 ± 0.038
6	2.020+07 ± 0.024	2.155+07 ± 0.068	3.577+08 ± 0.025
7	1.687+07 ± 0.030	2.080+07 ± 0.070	3.027+08 ± 0.041
8	1.867+07 ± 0.032	1.708+07 ± 0.061	3.537+08 ± 0.038
9	1.160+07 ± 0.025	1.483+07 ± 0.060	1.632+08 ± 0.034
10	1.191+07 ± 0.030	1.435+07 ± 0.072	1.737+08 ± 0.030
11	1.406+07 ± 0.032	1.785+07 ± 0.072	2.353+08 ± 0.044
12	3.337+07 ± 0.026	2.150+07 ± 0.052	6.320+08 ± 0.029
13	2.450+07 ± 0.019	2.370+07 ± 0.066	4.674+08 ± 0.024
14	2.397+07 ± 0.021	2.311+07 ± 0.051	4.702+08 ± 0.023
15	2.563+07 ± 0.026	2.114+07 ± 0.055	4.770+08 ± 0.030
16	1.915+07 ± 0.028	1.999+07 ± 0.109	3.529+08 ± 0.025
17	1.182+07 ± 0.034	1.221+07 ± 0.086	2.251+08 ± 0.030
18	2.988+07 ± 0.022	2.385+07 ± 0.052	5.783+08 ± 0.027
19	2.288+07 ± 0.028	1.915+07 ± 0.100	4.832+08 ± 0.032
20	2.230+07 ± 0.027	1.764+07 ± 0.057	5.098+08 ± 0.029
21	1.800+07 ± 0.029	2.220+07 ± 0.065	3.575+08 ± 0.030
22	1.101+07 ± 0.034	1.560+07 ± 0.115	2.292+08 ± 0.038
23	2.949+07 ± 0.024	2.585+07 ± 0.051	5.636+08 ± 0.032
24	2.219+07 ± 0.028	2.225+07 ± 0.083	4.627+08 ± 0.032
25	2.231+07 ± 0.027	1.959+07 ± 0.073	4.740+08 ± 0.032
26	1.619+07 ± 0.022	1.805+07 ± 0.068	3.095+08 ± 0.026
27	9.615+06 ± 0.031	1.010+07 ± 0.064	1.712+08 ± 0.034
28	2.790+07 ± 0.019	2.440+07 ± 0.057	5.446+08 ± 0.024
29	2.049+07 ± 0.022	1.616+07 ± 0.050	4.370+08 ± 0.025
30	1.905+07 ± 0.025	1.544+07 ± 0.046	4.114+08 ± 0.024
31	1.684+07 ± 0.021	1.816+07 ± 0.052	3.010+08 ± 0.029
32	9.686+06 ± 0.032	1.166+07 ± 0.082	1.707+08 ± 0.033
33	2.820+07 ± 0.021	2.276+07 ± 0.045	5.266+08 ± 0.027
34	2.046+07 ± 0.024	1.735+07 ± 0.047	4.502+08 ± 0.027

[a] A factor of 4π has already been included in these values.
[b] Read as 1.622×10^7.
[c] Fractional Standard Deviation.

Table 10 (Continued)

	Neutron	Secondary Gamma	Prompt Gamma
35	2.024+07 ± 0.023	1.591+07 ± 0.058	4.092+08 ± 0.026
36	4.341+05 ± 0.041	3.253+06 ± 0.049	9.931+06 ± 0.030
37	2.283+05 ± 0.049	7.196+05 ± 0.074	3.968+06 ± 0.052
38	2.433+05 ± 0.046	7.172+05 ± 0.149	3.812+06 ± 0.047
39	2.111+05 ± 0.038	5.367+05 ± 0.070	3.343+06 ± 0.041
40	1.391+05 ± 0.044	3.227+05 ± 0.095	1.931+06 ± 0.044
41	4.370+05 ± 0.040	3.445+06 ± 0.057	1.040+07 ± 0.030
42	2.415+05 ± 0.049	8.262+05 ± 0.072	4.097+06 ± 0.045
43	2.337+05 ± 0.045	7.316+05 ± 0.115	3.856+06 ± 0.038
44	2.139+05 ± 0.040	6.445+05 ± 0.084	3.370+06 ± 0.035
45	1.365+05 ± 0.042	3.171+05 ± 0.106	1.925+06 ± 0.036
46	1.193+08 ± 0.011	3.296+07 ± 0.065	2.739+09 ± 0.015
47	1.838+07 ± 0.028	1.185+07 ± 0.105	3.856+08 ± 0.030
48	1.492+07 ± 0.028	8.564+06 ± 0.113	3.208+08 ± 0.034
49	1.212+07 ± 0.030	5.906+06 ± 0.098	2.583+08 ± 0.032
50	7.344+06 ± 0.036	2.940+06 ± 0.102	1.859+08 ± 0.038
51	1.511+09 ± 0.023	5.048+07 ± 0.041	6.504+08 ± 0.021
52	9.057+08 ± 0.033	2.765+07 ± 0.044	3.655+08 ± 0.025
53	4.728+09 ± 0.015	7.303+07 ± 0.035	1.082+09 ± 0.016
54	3.269+09 ± 0.020	5.082+07 ± 0.036	8.789+08 ± 0.018
55	3.168+09 ± 0.016	4.942+07 ± 0.038	9.021+08 ± 0.018
56	1.562+09 ± 0.022	5.526+07 ± 0.036	6.334+08 ± 0.021
57	8.708+08 ± 0.029	3.039+07 ± 0.042	3.584+08 ± 0.027
58	4.787+09 ± 0.017	6.866+07 ± 0.031	1.103+09 ± 0.019
59	3.249+09 ± 0.020	4.986+07 ± 0.035	8.678+08 ± 0.018
60	3.212+09 ± 0.018	5.264+07 ± 0.031	8.636+08 ± 0.021
61	2.891+09 ± 0.019	1.379+08 ± 0.034	1.378+09 ± 0.016
62	2.820+09 ± 0.018	1.321+08 ± 0.025	1.373+09 ± 0.018
63	1.274+10 ± 0.010	3.504+08 ± 0.019	4.038+09 ± 0.011
64	1.258+10 ± 0.012	3.606+08 ± 0.018	4.066+09 ± 0.013
65	2.778+09 ± 0.020	1.363+08 ± 0.029	1.374+09 ± 0.018
66	2.807+09 ± 0.019	1.414+08 ± 0.032	1.429+09 ± 0.016
67	1.240+10 ± 0.010	3.602+08 ± 0.020	4.119+09 ± 0.012
68	1.253+10 ± 0.010	3.522+08 ± 0.017	4.067+09 ± 0.012

6. HYDRODYNAMIC RESPONSES OF MATERIALS FROM NUCLEAR WEAPON X–RAYS

As noted above, the detonation of a nuclear weapon in space will give rise to large quantities of radiation with approximately 75% being in the form of x–rays. When these x–rays impact the surface of a satellite or any of the external components of the system, an impulse loading will occur that induces large stresses and/or changes in material phase that may permanently or temporarily damage the satellite and components, thereby rendering the system incapable of functioning during engagements or otherwise carrying out its intended mission.

Calculations were carried out to determine the effects of x–radiation on beryllium mirror surfaces. It can be envisioned that these kinds of mirrors might be mounted on an SBI satellite or on a laser aiming satellite in the defensive weapon system architecture. A second series of calculations were performed to compare the HULL[15] and PUFF–TFT[16] hydrocodes in assessing the thermo–mechanical stresses induced in an aluminum slab by x–rays from an exo–atmospheric nuclear weapon detonation.

6.1 HYDRODYNAMIC RESPONSE OF A BERYLLIUM TARGET TO MONO–ENERGETIC X–RAYS

When beryllium mirror surfaces are machined, impurities are introduced that can effect the survivability of the mirror during interdiction by x–radiation. To determine the severity of the vulnerability, a series of calculations were performed wherein x–rays were assumed to be incident on the surfaces of a beryllium slab with bulk impurities, a beryllium slab with bulk impurities and 300A of surface impurities, and a beryllium slab with bulk impurities and 300A of surface impurities at three times the concentration of the previous case. Analyses were carried out for 1 and 2 keV blackbody x–rays incident on the mirror surface at wall loadings of 1 and 2 cal/cm^2. The radiation was incident in a square wave distribution having a duration of 5 n/sec. The complete details of the analysis are given in Ref. 6. In this document, only the 2 keV, 1 cal/cm^2 energy deposition and time dependent temperature change results are presented for the cases with and without surface impurities.

The energy deposition as a function of depth for the three configurations described above are shown in Figures 3–5. The impurity layer which contains ~15% trace elements of C, O, F, Al, Si, P, S, Cl, Cr, and Cu in various proportions, leads to a rapid attenuation of the incident x–rays with corresponding increase in the local energy deposition. For 2 keV incident x–radiation, ~23% leakage through the Be substrate occurs compared to 3% in the case of 1 keV radiation. Figures 6–8 show the corresponding temperature rises as a function of depth at different times after irradiation. For the source considered, the maximum temperature observed is ~250°C (for the triple impurity concentration), which is below the temperature threshold for damage for Be mirrors. However, for lower energy incident radiation, temperature excursions in excess of 5000°C will occur at 5 cal/cm^2 wall loadings and mirror surface damage is expected to occur.

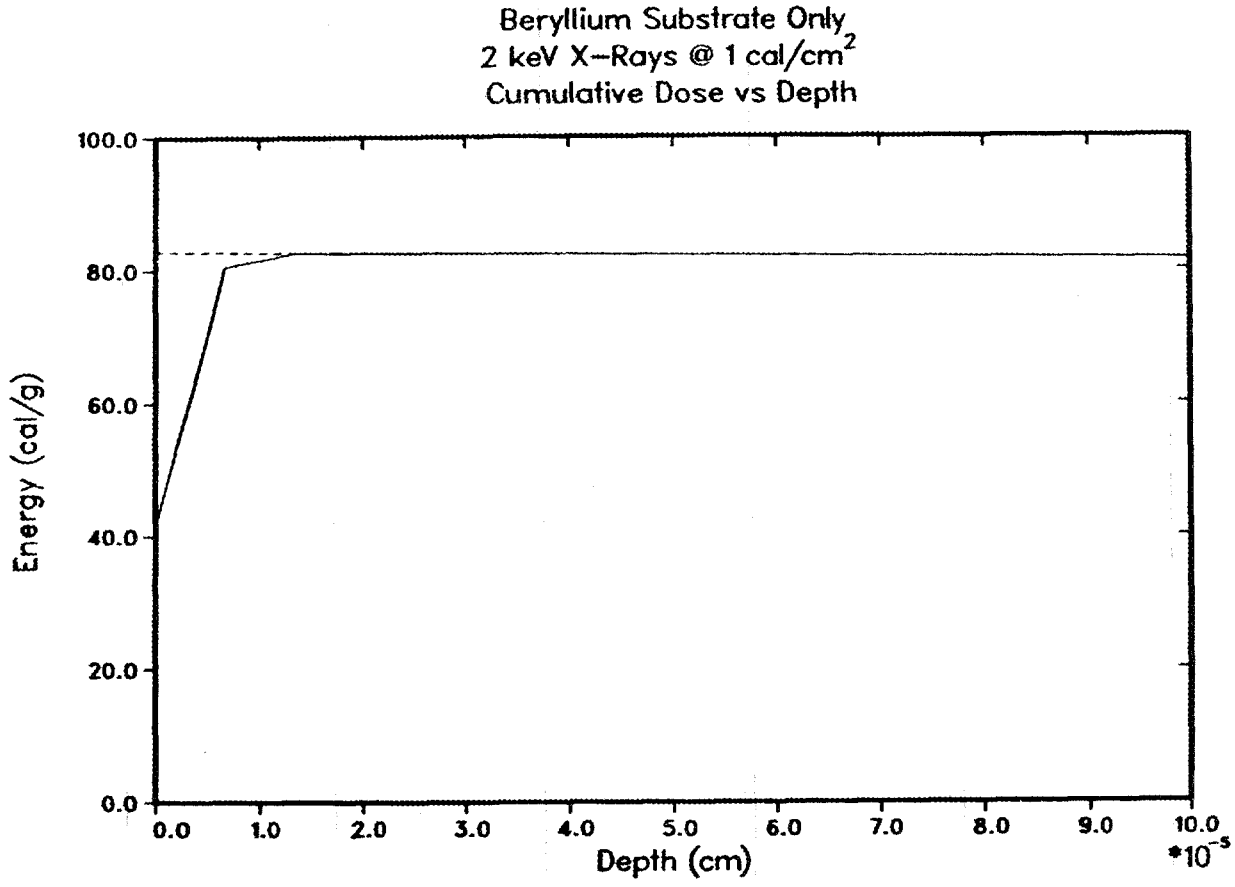

Figure 3. Energy deposited as a function of depth for the 2 keV, 1 cal/cm^2 source incident upon the beryllium substrate (no surface impurity layer).

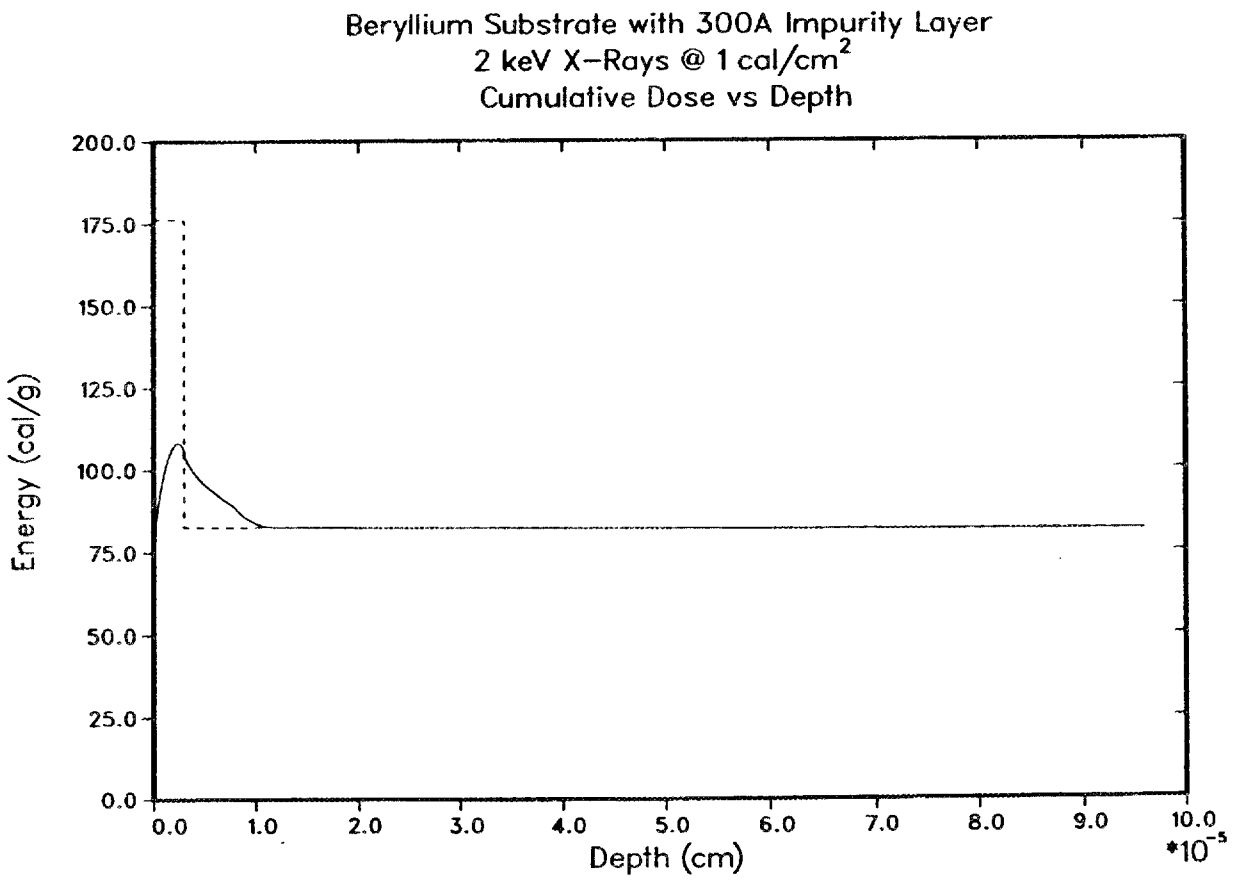

Figure 4. Energy deposited as a function of depth for the 2 keV, 1 cal/cm^2 source incident upon the 300 Å thick surface impurity layer with the base impurity concentrations.

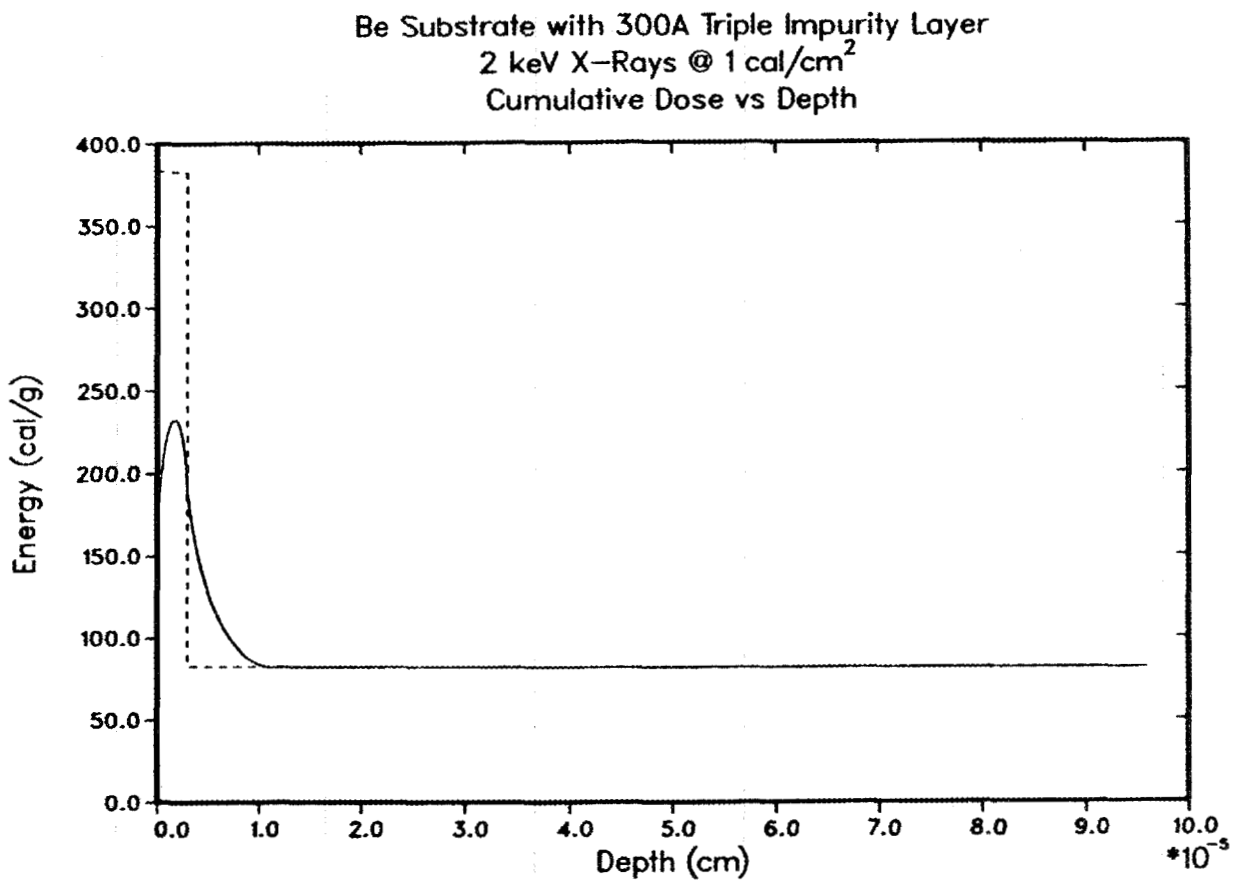

Figure 5. Energy deposited as a function of depth for the 2 keV, 1 cal/cm^2 source incident upon the 300 Å thick surface impurity layer with triple impurity concentrations.

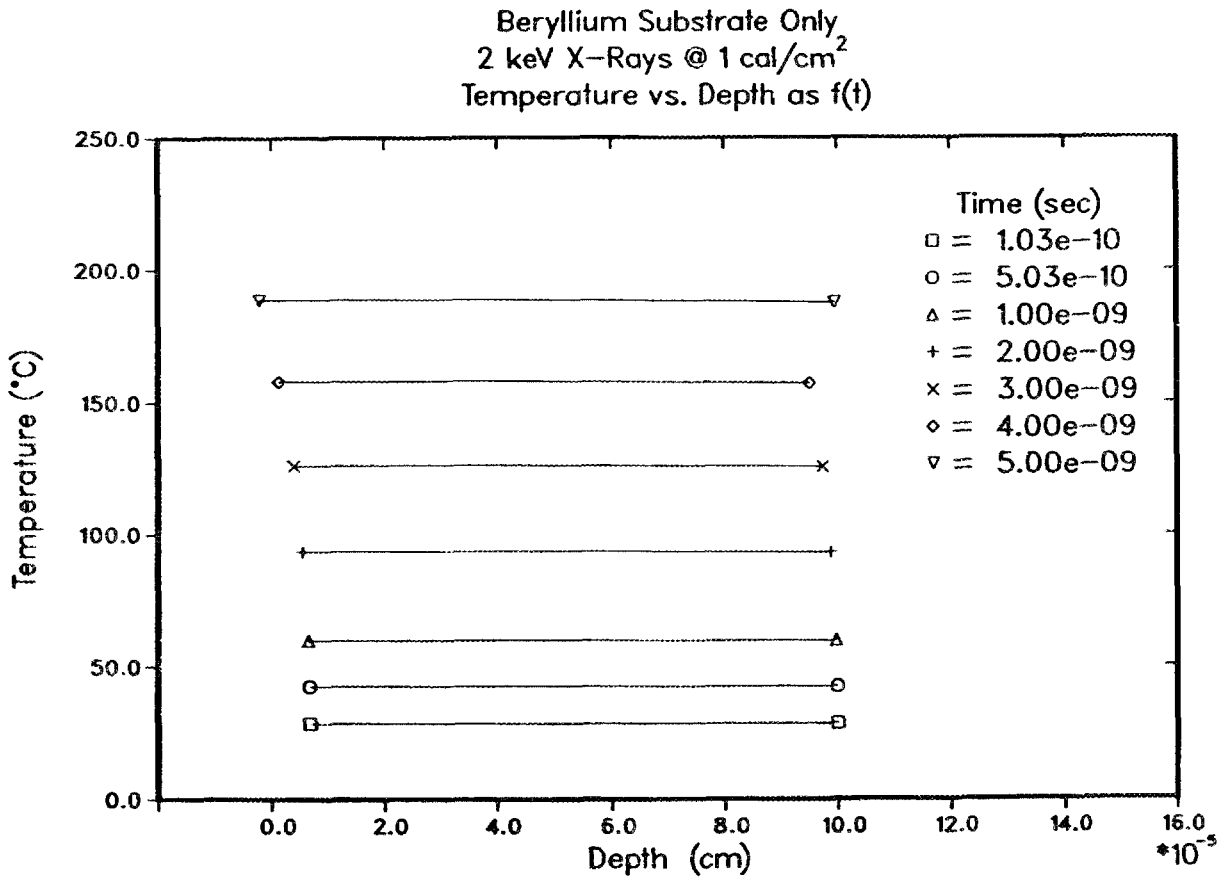

Figure 6. Temperature as a function of depth at specific times for the 2 keV, 1 cal/cm^2 source incident upon the beryllium substrate (no surface impurity layer).

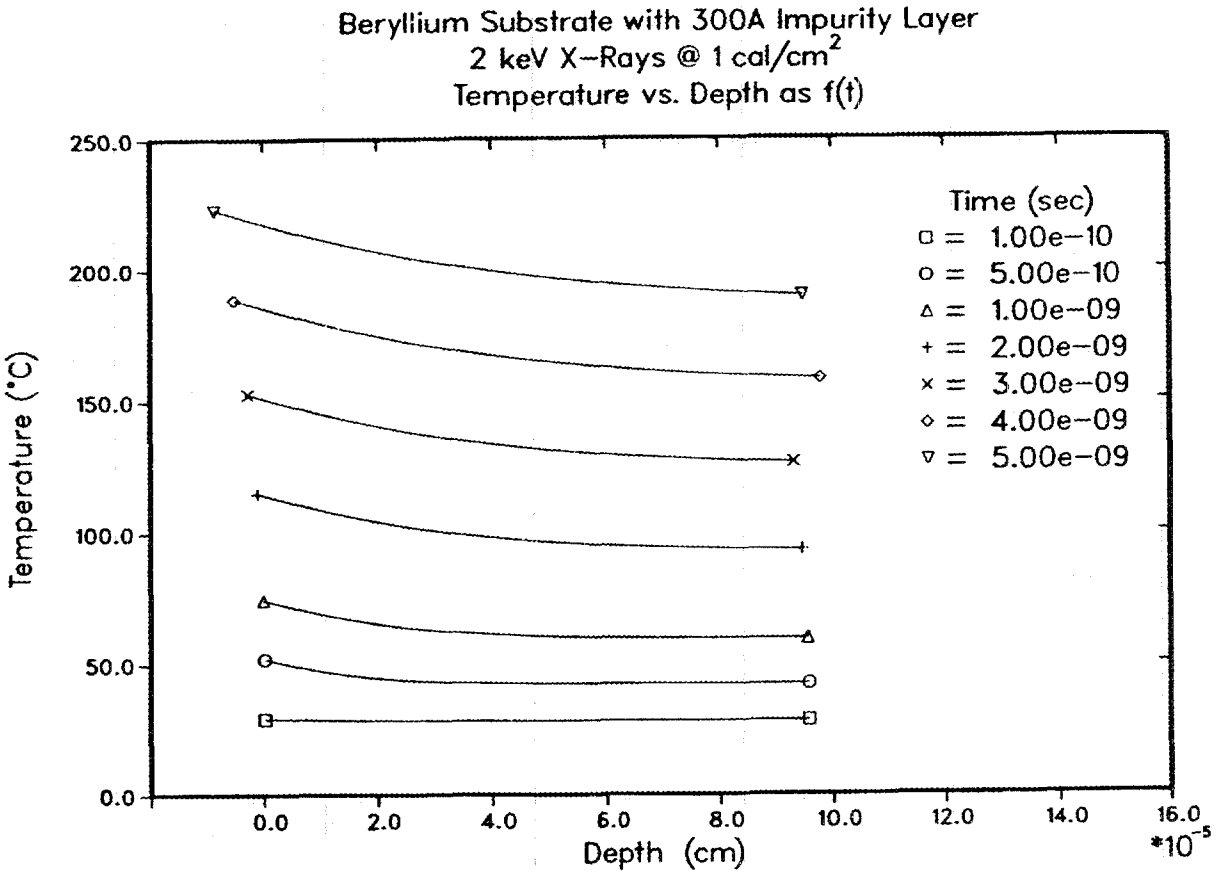

Figure 7. Temperature as a function of depth at specific times for the 2 keV, 1 cal/cm^2 source incident upon the 300 Å thick surface impurity layer with the base impurity concentrations.

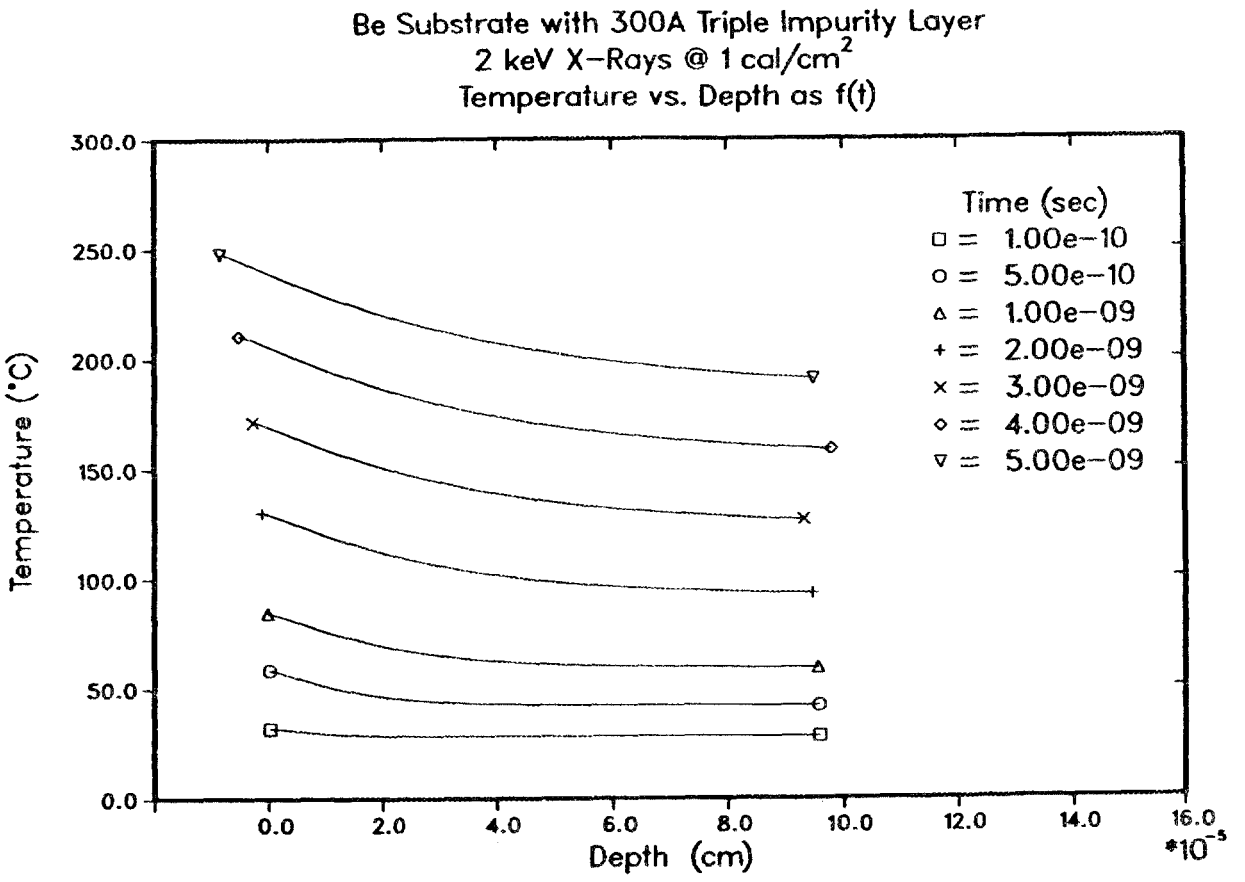

Figure 8. Temperature as a function of depth at specific times for the 2 keV, 1 cal/cm^2 source incident upon the 300 Å thick surface impurity layer with triple impurity concentrations.

6.2 COMPARISON OF THE THERMO–MECHANICAL RESPONSE OF AN ALUMINUM SLAB USING THE HULL AND PUFF–TFT CODES

Two hydrodynamic computer codes, HULL[15] and PUFF-TFT,[16] have been used to assess the thermo–mechanical response of an aluminum slab from incident X–rays characteristic of an exo-atmospheric nuclear detonation. A blackbody spectrum at 5 keV was normalized to yield a surface loading of approximately 90 cal/cm^2. This corresponds to a 1.5 Megaton detonation at a distance of 10 kilometers, assuming 75% of the energy is in the form of X–rays. The aluminum target was 0.16 cm thick, with a density of 2.71 g/cm^3.

For a detailed comparison of the two codes' capabilities, an examination was performed of the density, internal energy, axial stress, mass fractions of vapor, liquid, and solid phases, and fracture locations at six time intervals: 0.1, 0.2, 0.3, 0.5, and 1.0 μsecond was performed. In addition, the initial energy deposition was also examined. The energy deposition data at time=0.0 and the density, internal energy, and axial strength as a function of depth in the Al slab at time=0.1 μsec are presented here. The results obtained at other time intervals are given in Reference 5.

6.3 ENERGY DEPOSITION AT TIME = 0.0

The energy deposition calculations are performed for both codes prior to the initial time step. HULL uses the energy deposited from the EGS4 code[10] as an impulse. For the HULL code, the aluminum was subdivided into 64 uniform spatial grid points. PUFF computes the energy deposition from the blackbody spectrum and surface loading and allocates the energy over a specified time frame. PUFF employed an automatic zoning procedure that generated about twice as many mesh cells (nonuniform) as HULL. For this problem, all of the energy was deposited within 1 nanosecond. Figure 9 shows the energy deposition as a function of depth for each code. The calculated energy deposition as a function of depth is essentially identical for the two codes. The calculated error for EGS is within $\pm 10\%$ ($\pm 1\sigma$).

From the energy deposition, the PUFF code flags those cells that have vaporized or melted. Cell masses are summed and mass fractions computed for each phase. A rough estimate of the mass fractions in each phase can be made for HULL from the initial internal energy. Table 11 lists the calculated mass fraction by phase for each code at time = 0.0. If it is assumed the two phase regions in the HULL calculations are equally proportioned between the solid/liquid and liquid/vapor phases, excellent agreement is obtained with PUFF *i.e.*, for HULL, half of the two phase liquid/solid region can be added to the liquid only portion to yield $\approx 22\%$, in reasonable agreement with PUFF.

6.4 COMPARISON OF RESULTS AT TIME = 0.1μsec.

Figures 10–12 compare density, internal energy, and axial stress as a function of depth. Included with the plot of density are vertical dashed lines denoting fracture locations as predicted by PUFF. Similarly, phase transitions are marked on the plot of internal energy. These conventions will be continued throughout this analysis.

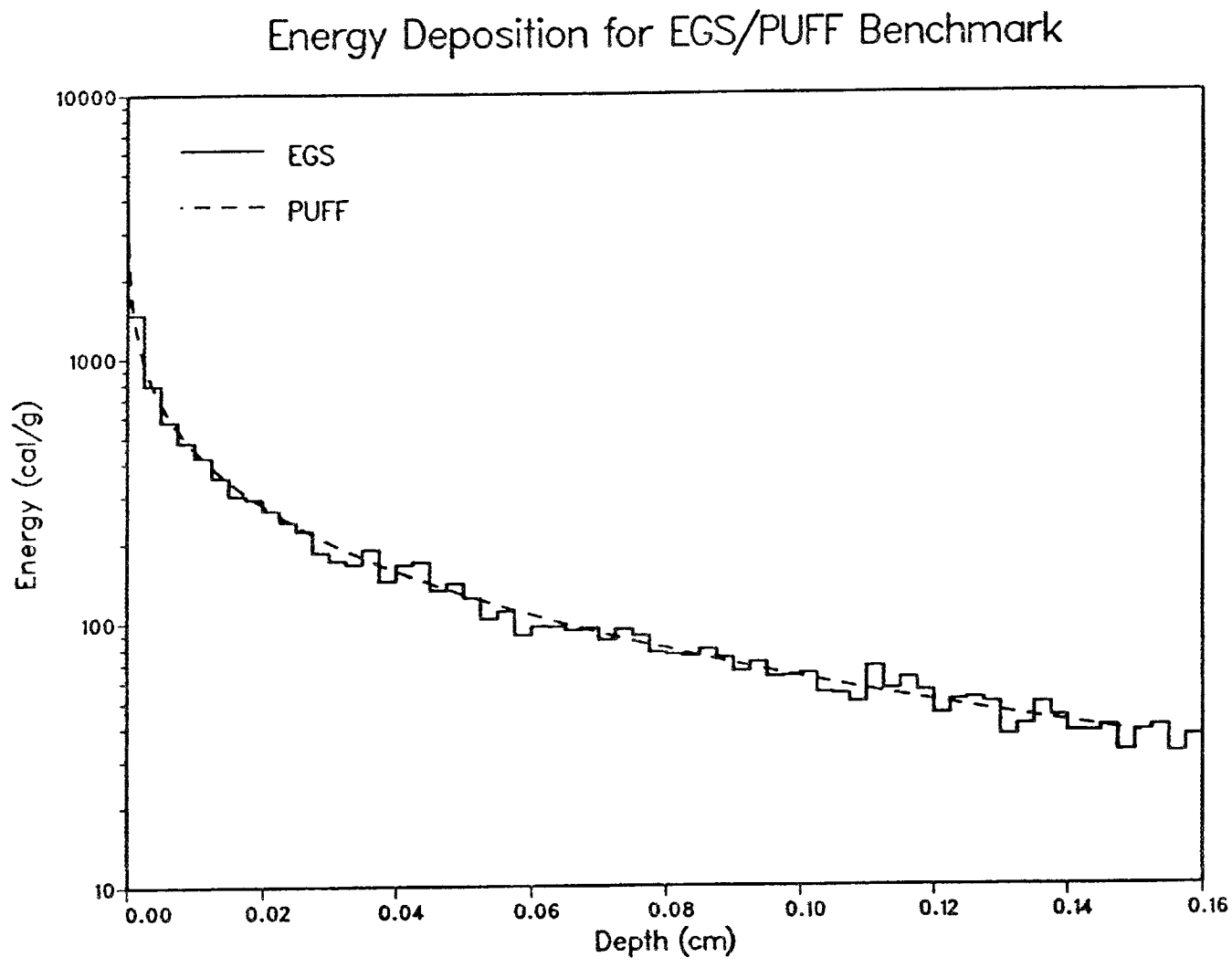

Figure 9. Energy deposition as a function of depth.

Table 11
Approximate Mass Fractions by Phase

	PUFF	HULL
Vapor	2.5%	
2ϕ		3%
Liquid	21.5%	min. 14%
2ϕ		16%
Solid	76.0%	min. 67%

A close examination of Figure 10 reveals several interesting features. First it is noted that the ablation wave front from PUFF is much greater than that from HULL. This is not surprising due to the difference in boundary conditions, *i.e.*, vacuum (PUFF) vs. air (HULL). Both codes are in agreement as to the solid density, although PUFF predicts a small increase in density at the location of peak axial stress (see Figure 12). Both codes also predict a density spike which occurs for PUFF at the vapor/liquid interface. This liquid wave front is beginning to separate from the remaining material according to the HULL code. The PUFF code shows early fracture locations at the liquid/solid interface.

The plots of internal energy (Figure 11) are in good agreement. Here also PUFF calculates a small increase in internal energy at the peak axial stress location. The rapid expansion of the ablated material is again evident from the PUFF results. An attempt was made to correct one of the many differences in the two codes: HULL includes an ambient component in its internal energy, *i.e.*, at 300 K, the internal energy of aluminum is about 60 cal/g. This was added to the PUFF value for this comparison. Figure 12 compares axial stress. Although both codes agree on the location of the peak stress, there is a considerable difference in the magnitude. This difference cannot be explained at this time, although efforts are underway to achieve this.

Both computer codes calculated extreme damage levels in the aluminum slab. Although there was considerable disagreement in the magnitude of the axial stress before the compressive wave reflected off the back surface and differences in shape after reflection, the end result for both codes was markedly similar. Density as a function of depth, fracture locations and times, and mass fractions were all equivalent. The internal energy compared well at earlier times, but less favorably at later times. Some differences are to be expected, but the prediction of the magnitude of the axial stress needs to be more thoroughly investigated. Overall the PUFF code compared well with the more complex HULL model at a fraction of the cost.

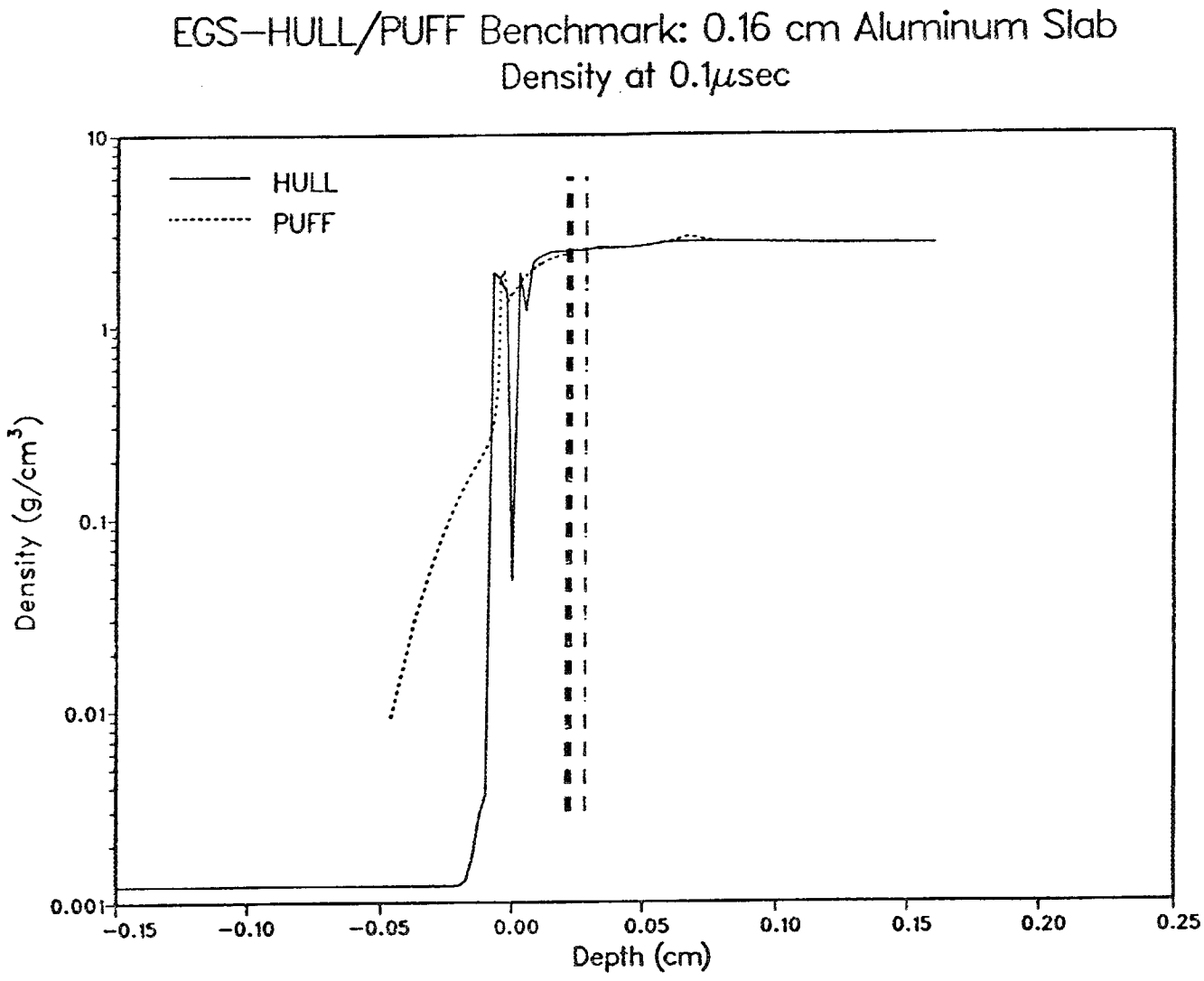

Figure 10. Density as a function of depth at 0.1μsec. Vertical dashed lines denote fracture locations.

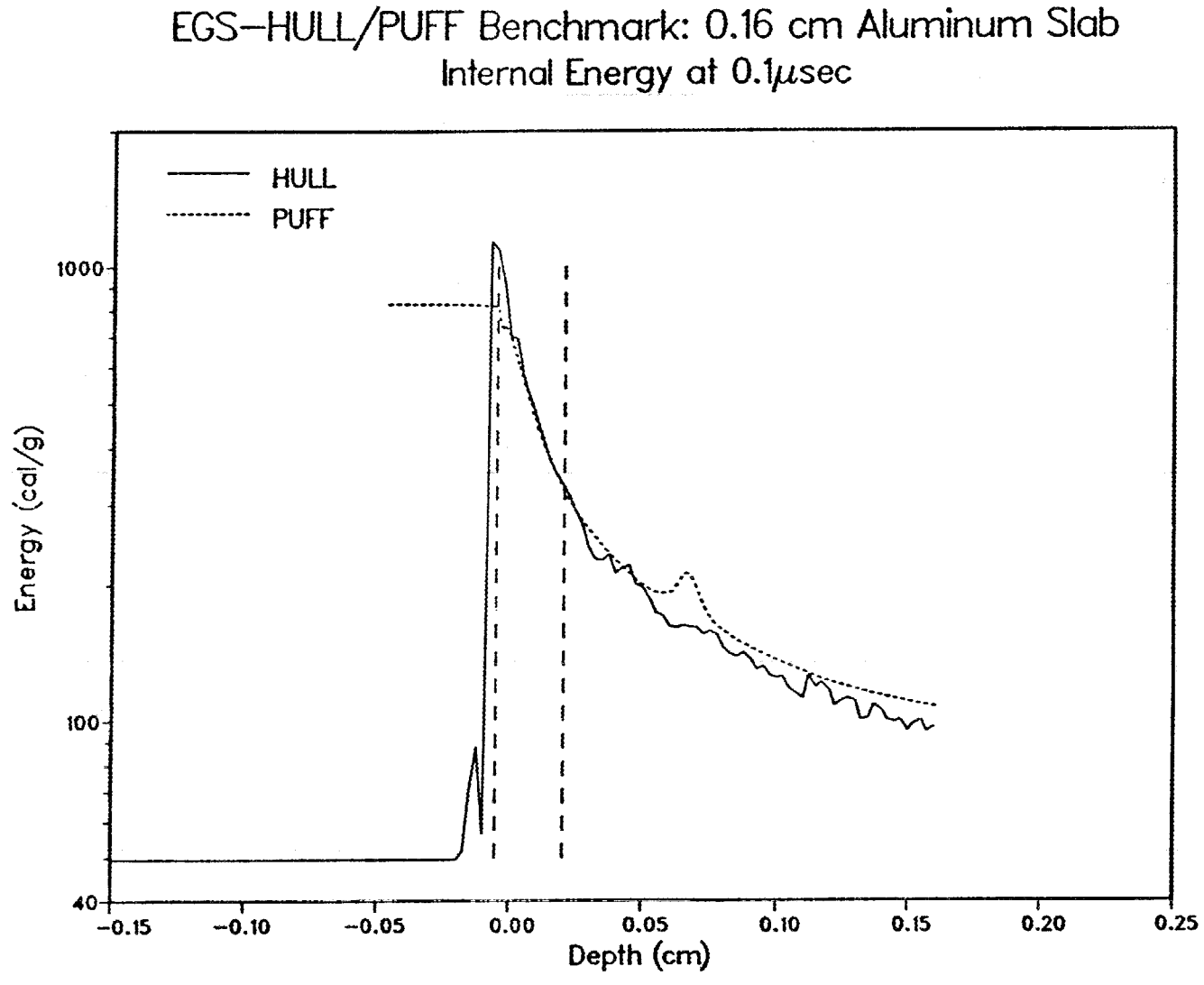

Figure 11. Internal energy as a function of depth at 0.1μsec. Vertical dashed lines denote phase transitions.

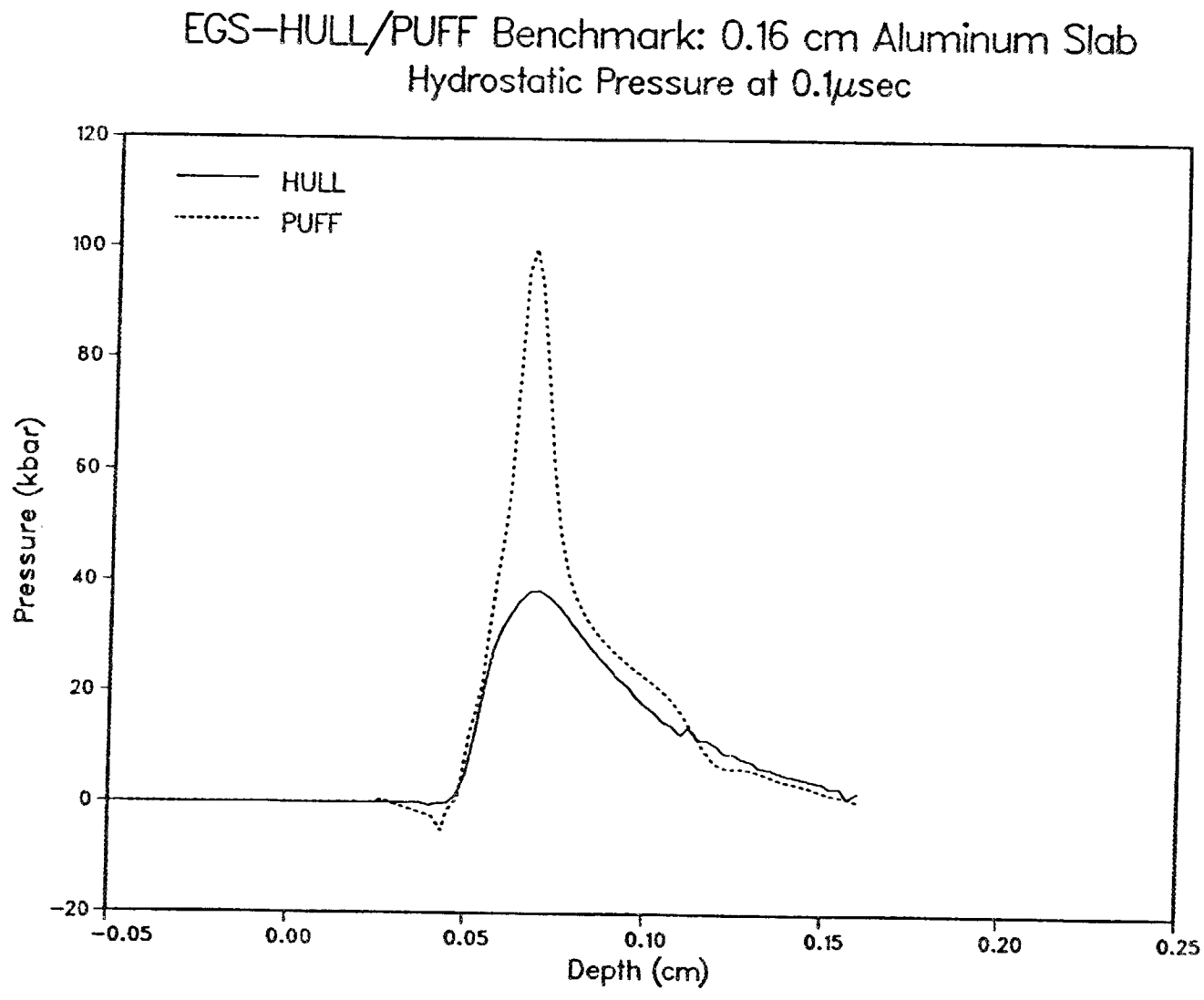

Figure 12. Hydrostatic pressure versus depth at 0.1μsec.

7. CONCLUSIONS

The work summarized here was carried out principally to determine the magnitude of the radiation damage in selected critical components of a prototypic space deployed SDI weapon system and to develop additional tools for estimating the effects of x–radiation impulse loadings on the surfaces of the satellite and external components. No attempt was made to optimize the locations of critical components or to add additional shielding to further reduce the effects of the natural and enhanced Van Allen belt radiation or the radiation from nuclear weapon detonations. These optimization studies were originally proposed as a follow–on study which, unfortunately, will not be done due to termination of the program funding because of a redirection of the SDI objectives for hardening these kinds of weapon platforms.

The estimates of the radiation damage from Van Allen belt radiation was shown to be small for deployment of the satellite at 500 km. Current plans call for deployment of surveillance satellites at higher altitudes than that studied here where the effects of trapped proton and electron radiation will be considerably more severe. The long–term radiation damage to essential components in these satellites must be resolved prior to deployment to assure that on–board systems will be functional over the mission lifetime of the system.

Assessment of the long–term natural radiation and transient effects from exploding weapons should be continued to satisfactorily identify requirements for specific additional component shielding or to more fully resolve keep–out distances.

REFERENCES

1. R. T. Santoro and T. A. Gabriel, "Executive Summary, The Oak Ridge National Laboratory Strategic Defense Initiative Shield Optimization Program," ORNL/TM–10629, Oak Ridge National Laboratory, (April 1988). Also refer to T. A. Gabriel, J. M. Barnes, B. L. Bishop, J. D. Drischler, J. O. Johnson, R. A. Lillie, R. T. Santoro, and M. S. Smith, "The Oak Ridge National Laboratory Strategic Defense Initiative Shield Optimization Program," ORNL/TM–10631, Oak Ridge National Laboratory, (April 1988).

2. J. M. Barnes, R. T. Santoro, J. O. Johnson, J. D. Drischler, T. A. Gabriel, and M. S. Smith, "Shield Optimization Program, Part II: Effects of Van–Allen Belt Radiation on SDI Weapon Platforms," ORNL/TM–10957, Oak Ridge National Laboratory, (December 1988).

3. J. O. Johnson, T. A. Gabriel, J. M. Barnes, J. D. Drischler, M. S. Smith, and R. T. Santoro, "Shield Optimization Program, Part III: Effects of X–Ray Radiation from Nuclear Weapons on SDI Weapons Platforms," ORNL/TM–10985, Oak Ridge National Laboratory, (March 1989).

4. M. S. Smith, J. O. Johnson, T. A. Gabriel, J. M. Barnes, J. D. Drischler, and R. T. Santoro, "Shield Optimization Program, Part IV: Effects of Neutron and Gamma–Ray Radiations on SDI Weapon Platforms," ORNL/TM–10975, Oak Ridge National Laboratory, (March 1989).

5. M. S. Smith, T. J. Burns, and J. O. Johnson, "Shield Optimization Program, Part V: A Hydrodynamic Comparison using HULL and PUFF–TFT for a One-Dimensional Aluminum Slab," ORNL/TM–11160, Oak Ridge National Laboratory, (April-1989).

6. M. S. Smith, S. McNeany, R. T. Santoro, and T. A. Gabriel, "Shield Optimization Program, Part VI: The Effects of Impurity Layers on the Hydrodynamic Response of a Beryllium Target to Mono–Energetic X–Rays using the PUFF–TFT Code," ORNL/TM–11038, Oak Ridge National Laboratory, (March 1989).

7. T. A. Gabriel, "The High Energy Transport Code HETC," ORNL/TM-9727, Oak Ridge National Laboratory, (September 1985).

8. M. B. Emmett, "MORSE–CGA, A Monte Carlo Radiation Transport Code with Array Geometry Capability," ORNL–6174, Oak Ridge National Laboratory, (April 1985).

9. J. O. Johnson and T. A. Gabriel, "Development and Evaluation of a Monte Carlo Code System for Analysis of Ionization Chamber Responses," ORNL/TM–10196, Oak Ridge National Laboratory, (December 1985).

10. Walter R. Nelson, Hideo Hirayama, and David W. O. Rogers, "The EGS4 Code System," SLAC–265, (December 1985).

11. M. B. Emmett, L. M. Petrie, and J. T. West, "JUNEBUG–11 – A Three Dimensional Plotting Code," NUREG/CR–0200, Volume 2, Section F12, ORNL/NUREG–CSD–2/V2/R, (December 1984).

12. DC. E. McIllwain, "Coordinates for Mapping Magnetically Trapped Particles," *J. Geophys. Research* **66**, 3681, (1968).

13. CPT Roman B. Zarcharko, "High Altitude Nuclear Burst Electron Fluence and Dose Calculations for a Parametric Set of Orbits," External Correspondence, Air Force Weapons Laboratory, Kirtland Air Force Base, New Mexico.

14. R. Siegal and John R. Howell, "Thermal Radiation Heat Transfer," McGraw–Hill, Inc., 1972.

15. A.J. Watts, C. Breen, S. Sauer, and F. Smith, "Thin Film Transport (PUFF–TFT) Computer Code Development," AFWL–TR–88–66, Parts 1 and 2, Air Force Weapons Laboratory, Kirtland AFB, NM, June 1988.

16. D. A. Matuska, and J. J. Osborn, "The HULL Code System," Orlando Technology, Inc., Shalimar Fla. (1983).

INTERNAL DISTRIBUTION

1. R. G. Alsmiller, Jr.
2. B. R. Appleton
3. D. E. Bartine
4. J. M. Barnes
5. T. J. Burns
6. R. M. Davis
7. J. B. Dooley
8. J. D. Drischler
9–13. T. A. Gabriel
14. C. M. Haaland
15. E. B. Harris
16. D. T. Ingersoll
17. J. O. Johnson
18. R. A. Lillie
19. F. C. Maienschein
20. S. McNeany
21. J. R. Merriman
22. W. L. Roberts
23. R. W. Roussin
24–28. R. T. Santoro
29. M. S. Smith
30. D. G. Thomas
31. R. C. Ward
32. C. R. Weisbin
33. EPMD Reports Office
34–35. Laboratory Records Department
36. Laboratory Records, ORNL-RC
37. Document Reference Section
38. Central Research Library
39. ORNL Patent Section

EXTERNAL DISTRIBUTION

40. Dr. Charles Aeby, AFWL/NTC, Air Force Weapons Laboratory, Kirtland Air Force Base, New Mexico 87117-6008
41. Lt Dale Atkinson, AFWL/NTCA, Air Force Weapons Laboratory, Kirtland Air Force Base, New Mexico 87117-6008
42. Richard Bradshaw, U.S. Army Strategic Defense Command, 106 Wynn Drive, Huntsville, Alabama 35805
43. J. J. Dorning, Department of Nuclear Engineering and Engineering Physics, Thornton Hall, University of Virginia, Charlottesville, Virginia 22901
44. Lt Richard Engstrom, AFWL/NTCA, Air Force Weapons Laboratory, Kirtland Air Force Base, Albuquerque, New Mexico 87117
45. R. M. Haralick, Department of Electrical Engineering, University of Washington, Seattle, Washington 98195
46. Phil Jessen, Mission Research Corp., 4935 N. 30 Street, Colorado Springs, Colorado 80919
47. Claud Martin, U.S. Army Strategic Defense Command, 106 Wynn Drive, Huntsville, Alabama 35805

48–52. Paul Sonnenburg, Physicon, Inc., 3325 Triana Blvd., Suite A, Huntsville, Alabama 35805

53. John Tinsley, Kaman Sciences Corp., 1500 Garden of the Gods Road, Colorado Springs, Colorado 80907
54. Office of the Assistant Manager for Energy Research and Development, Department of Energy, Oak Ridge Operations, P.O. Box 2001, Oak Ridge, TN 37831

55–64. Office of Scientific and Technical Information, P.O. Box 62, Oak Ridge, Tennessee 37830